International Journal of Rock Mechanics & Mining Sciences 152 (2022) 105061

Contents lists available at ScienceDirect

International Journal of Rock Mechanics and Mining Sciences

journal homepage: www.elsevier.com/locate/ijrmms

Combined effect of anisotropy and uncertainty on the safe mud pressure window of horizontal wellbore drilled in anisotropic saturated rock

Nam Hung Tran [a], Duc Phi Do [b,*], Minh Ngoc Vu [c,d], Thi Thu Nga Nguyen [a], Duc Tho Pham [e], Hung Truong Trieu [e]

[a] Le Quy Don Technical University, Institue of Technique for Special Engineering, Hanoi, Viet Nam
[b] Univ Orléans, Univ Tours, INSA CVL, Lamé, EA, 7494, France
[c] Division of Construction Computation, Institute for Computational Science, Ton Duc Thang University, Ho Chi Minh City, Viet Nam
[d] Faculty of Civil Engineering, Ton Duc Thang University, Ho Chi Minh City, Viet Nam
[e] Hanoi University of Mining and Geology, Hanoi, Viet Nam

ARTICLE INFO

Keywords:
Safe mud pressure window
Horizontal wellbore
Anisotropic rock
Sensitivity analysis
Stochastic analysis
Monte Carlo simulation
Kriging metamodeling technique

ABSTRACT

The investigation of safe mud pressure window of horizontal wellbore drilled in the saturated rock by accounting for the combined effect of anisotropy and uncertainty is the main purpose of this work. To this aim, the deterministic solution of collapse and fracture initiation pressures are firstly presented in three cases that describe the behavior of wellbore: (1) immediately after drilling (i.e., undrained problem); (2) at long term due to the steady-state fluid flow (permeable boundary case) and (3) by neglecting the variation of initial pore pressure (i.e., impermeable boundary condition case). Based on these deterministic solutions, the key parameters of different sources of anisotropy (initial stress state, poro-elastic and strength properties of rock mass) are highlighted through sensitivity analysis. Then, the famous Monte Carlo Simulation (MCS) is undertaken to quantify the uncertainty effect on the probability of success of safe mud pressure window of the wellbore. We also present an adaptation of the Kriging metamodeling technique to study the stability of wellbore. In comparison with the referent solution of MCS, the Kriging metamodel provides a high accuracy and can be used as a performant tool for the probabilistic assessment of wellbore. The consideration of anisotropy combined with uncertainty, and the hydraulically boundary condition around wellbore in this work allows us to complete the contributions in the literature and confirm their strong effect on the design of wellbore.

1. Introduction

The accurate prediction of safe mud pressure window is the most important task in wellbore design. Traditionally, the estimation of mud weights to ensure the stability of wellbore against shear and tensile failure is widely undertaken under the hypothesis of isotropic behavior of geological rock formation. In addition, collapse and fracture initiation pressures in the wellbore result from the deterministic calculation with the fixed values of input data.[1–3]

It has been shown in many works that the anisotropic behavior of rocks (e.g., sedimentary and metamorphic foliated rock) can significantly affect the distribution of stress state around the wellbore.[4–8] For example, Aadnoy[9] and then Hefny and Lo[10] determined the stress state around the horizontal borehole drilled in transversely isotropic rock by using the complex stress functions of Lekhnitskii.[11,12] The problem is then extensively considered in the more general case of inclined wellbore drilled in the anisotropic rock (see Refs. 13,14 and references therein) based on the Lekhnitskii-Amadei solution.[15] These studies highlighted the strong dependence of stress state and hence of the safe mud pressure window on the elastic properties of anisotropic rocks. Furthers, the anisotropy of tensile and shear strengths of rocks also presents an essential role on the stability of the wellbore.[13,14,16–18] Especially, in the bedded rocks like shale, the strength of planes of weakness can be the critical parameter. Combined with the wellbore inclinations and the three-dimensional stress state, the effect of weak planes may lead to severe collapse of the wellbore.[13,16,17] In their work, Setiawan and Zimmerman[14] demonstrated the pronounced effect of plane of weakness as well as the intermediate stress on the wellbore stability by using the both well-known Mogi-Coulomb and Jeager models as failure criteria of intact rock and the bedding plane.

* Corresponding author.
E-mail address: duc-phi.do@univ-orleans.fr (D.P. Do).

https://doi.org/10.1016/j.ijrmms.2022.105061
Received 26 August 2021; Received in revised form 23 January 2022; Accepted 15 February 2022
Available online 25 February 2022
1365-1609/

Whilst most the contributions as cited above focus in the case of dry rock, the effect of pore pressure in the anisotropic saturated rock has been recently received more attention. For instance, in their work, Do and his co-workers used the well-known complex potential approach to derive the closed-form solution of effective stresses around the wellbore drilled in the transversely isotropic poro-elastic rock.[19–22] Unlike the case of the wellbore in isotropic rock, the explicit expressions of effective radial and tangential stresses depend on the poro-elastic properties of anisotropic rock. Consequently, in the application of wellbore design, Do et al.[7,8] pointed out that the anisotropic poro-elastic properties of rock mass combined with the anisotropy in the in-situ stress state and that in the tensile and shear strengths, result in the remarkable difference of mud pressure windows in comparison with ones calculated from the isotropic rock. Furthermore, the hydraulic boundary prescribed on the borehole wall can also present a pronounced impact on the collapse and fracture pressures in the wellbore.

The heterogeneous characteristic in nature and the lack of knowledge related to the limitation test data induce the inherent uncertainty in rock properties. Therefore, there is an increasing interest in modeling of uncertainties propagation on the stability and optimization design of the underground structure in rock engineering.[23–25] In petroleum application, the stochastic analysis has been intensively considered to assess the optimal mud pressure windows by accounting for the uncertainty of input data like in-situ stress state, initial pore pressure, and strength properties of the surrounding rock. For example, several studies used the quantitative risk assessment to study the stability and optimize the mud weight windows.[26–29] The Monte Carlo Simulation (MCS) has been generally chosen in these previous studies to quantify the uncertainties and the associated probability of success in wellbore collapse and lost circulation pressures.[30–37] However, to the best of the authors' knowledge, the entire stochastic assessment of wellbore has been limited in the case of isotropic rocks.

The aim of this work consists in assessing the safe mud pressure windows of the horizontal wellbore drilled in anisotropic saturated rock by accounting for the uncertainty combined with anisotropy of input data including the anisotropic in-situ stress, anisotropic poro-elastic properties, as well as the anisotropic strengths of rock mass.

In the following, the paper will be organized into three main parts. Firstly, the deterministic solution of safe mud pressure windows derived from the closed-form solution of stress state around the horizontal wellbore for the chosen tensile and shear failure of anisotropic poro-elastic rock is shown. Then, the sensitivity analysis and the probabilistic assessment based on the MCS are undertaken by accounting for the uncertainty of different anisotropic sources. An adaptation and validation of the well-known Kriging metamodeling technique for the stability analysis of such wellbore are also presented in this section. Essential conclusions are finally made from the results drawn throughout the manuscript.

2. Tensile and collapse pressures of horizontal wellbore in transversely isotropic rock

In this section, the deterministic solution of the tensile and collapse pressures of the horizontal wellbore drilled in the transversely isotropic rock with a vertical axis of symmetry (VTI) is briefly presented. The solution of this deterministic problem is key issue to conduct the probabilistic analysis using the MCS.

2.1. Closed-form solution of stress state around wellbore in transversely isotropic saturated rock

Considering a circular horizontal wellbore drilled in a transversely isotropic poro-elastic rock, with the assumption that the longitudinal axis of the wellbore lies on the horizontal plane and coincides with one principal horizontal stress axis as shown in Fig. 1a. The angle between the normal to the bedding plane and the principal vertical stress is β

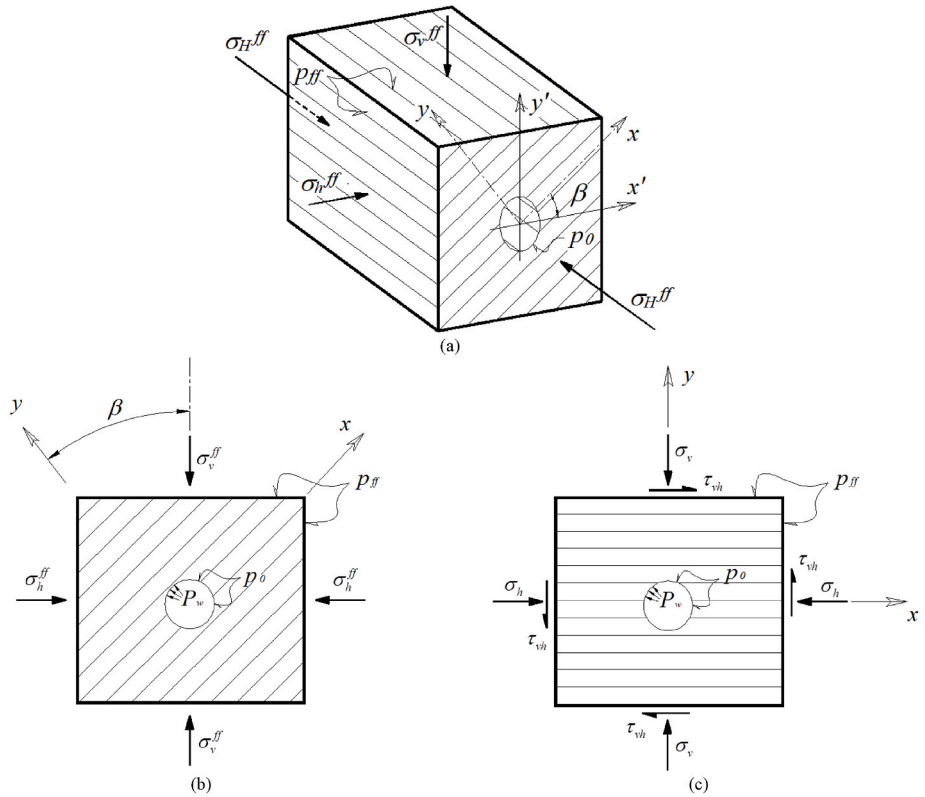

Fig. 1. Geometry of horizontal wellbore drilled in transversely anisotropic formation (a) whose bedding plane inclined an angle β with the principal stress axis at the far-field (b), equivalent problem after the rotation (c).

(Fig. 1b). The rock formation around the wellbore is saturated with an initial pore pressure p_{ff} whilst the mud pressure in wellbore P_w acts as radial stress on the wall of the wellbore. In the case of highly permeable rock, the mud pressure can also act as pore pressure on the well wall.[7,38] Thus, by noting p_0 as the pore pressure on the circumference of the wellbore, we have $p_0 = p_{ff}$ if the variation of pore pressure is neglected (called as impermeable boundary case of wellbore) while $p_0 = P_w$ if the boundary of wellbore is permeable.[7]

Adopting the 2D plane strain hypothesis (i.e., the component $\varepsilon_z, \varepsilon_{xz}$ and ε_{yz} vanish everywhere), this initial problem can be transformed into the equivalent problem in the symmetric coordinate system of the VTI medium (Fig. 1c). In this 2D plane strain equivalent problem, the far-field stress reads:

$$\begin{aligned}\sigma_v &= \frac{1}{2}(1+K_0)\sigma_v^{ff} + \frac{1}{2}(1-K_0)\sigma_v^{ff}\cos 2\beta,\\ \sigma_h &= \frac{1}{2}(1+K_0)\sigma_v^{ff} - \frac{1}{2}(1-K_0)\sigma_v^{ff}\cos 2\beta,\\ \tau_{vh} &= \frac{1}{2}(1-K_0)\sigma_v^{ff}\sin 2\beta,\end{aligned} \tag{1}$$

with. $K_0 = \sigma_h^{ff}/\sigma_v^{ff}$

The determination of the stress state around the wellbore consists in solving the following differential equations:

- The 2D plane strain equilibrium equation:

$$\frac{\partial \sigma_x}{\partial x} + \frac{\partial \tau_{xy}}{\partial y} = 0, \quad \frac{\partial \tau_{yx}}{\partial x} + \frac{\partial \sigma_y}{\partial y} = 0, \tag{2}$$

- The strain compatibility equation:

$$2\frac{\partial^2 \varepsilon_{xy}}{\partial x \partial y} = \frac{\partial^2 \varepsilon_x}{\partial y^2} + \frac{\partial^2 \varepsilon_y}{\partial x^2}, \tag{3}$$

where the Hooke's law written in 2D plan strain conditions is:

$$\begin{pmatrix}\varepsilon_x\\ \varepsilon_y\\ \varepsilon_{xy}\end{pmatrix} = \begin{pmatrix}s_{11} & s_{12} & 0\\ s_{21} & s_{22} & 0\\ 0 & 0 & s_{33}\end{pmatrix}\begin{pmatrix}\sigma_x'\\ \sigma_y'\\ \tau_{xy}'\end{pmatrix}, \tag{4}$$

- The fluid flow in the porous rock is characterized by the diffusion equation:

$$k_x\frac{\partial^2 p}{\partial x^2} + k_y\frac{\partial^2 p}{\partial y^2} = \gamma_w\frac{\partial \chi}{\partial t}, \tag{5}$$

where k_x and k_y are hydraulic conductivities in the horizontal x-direction and vertical y-direction respectively and γ_w is the unit weight of the pore fluid. The variation of fluid volume per unit volume of the porous material χ is defined as:

$$\chi = \frac{p}{M} + (\alpha_x\varepsilon_x + \alpha_y\varepsilon_y), \tag{6}$$

where the parameter M is the well-known Biot's modulus whilst the second term in brackets presents change of fluid volume due to volumetric strain by accounting for the mechanical effect.

In Eq. (4), the notion of effective stress based on the Biot's theory is used to characterize the influence of the pore pressure on the mechanical response:

$$\sigma_x' = \sigma_x + \alpha_x p, \quad \sigma_y' = \sigma_y + \alpha_y p, \tag{7}$$

with σ', σ are respectively the effective and the total stresses; α_x, α_y are the Biot coefficients in the horizontal and vertical directions. Herein, we note that the tensile stress and pressure are considered positive.

The compliance coefficients $(s_{11}, s_{12}, s_{21}, s_{22}, s_{33})$ in Eq. (4) and the Biot coefficients are calculated from the five independent elastic parameters of transversely isotropic rock which are respectively: the horizontal and vertical Young's moduli (E_x E_y), the Poisson's ratios in the isotropic plane and anisotropic plane (ν_{xz} ν_{yx}) and the shear modulus G_{xy} in the anisotropic plane:

$$\begin{aligned}&s_{11} = \frac{1-\nu_{xz}^2}{E_x}, \quad s_{12} = s_{21} = -\frac{\nu_{xy}(1+\nu_{xz})}{E_x}, \quad s_{22} = \frac{1-\nu_{xy}\nu_{yx}}{E_y}, \quad s_{33} = \frac{1}{G_{xy}}, \quad \nu_{yx} = \nu_{xy}k_E, \quad k_E = \frac{E_y}{E_x};\\ &\alpha_x = 1 + \frac{E_xE_y(1+\nu_{yx})}{3K_s\left[2E_x\nu_{yx}^2 - E_y(1-\nu_{xz})\right]} = 1 - \frac{k_EE_x(1+\nu_{yx})}{3K_s\left[k_E(1-\nu_{xz}) - 2\nu_{yx}^2\right]},\\ &\alpha_y = 1 + \frac{E_y(E_y - E_y\nu_{xz} + 2E_x\nu_{yx})}{3K_s\left[2E_x\nu_{yx}^2 - E_y(1-\nu_{xz})\right]} = 1 + \frac{(1-\alpha_x)\left[k_E(1-\nu_{xz}) + 2\nu_{yx}\right]}{(1+\nu_{yx})},\end{aligned} \tag{8}$$

Note that the independent elastic parameters of the transversely isotropic rock verify the following thermodynamic conditions:

$$k_E(1-\nu_{xz}) - 2\nu_{yx}^2 > 0, \tag{9}$$

So far, the derivation of the analytical resolution for the anisotropic poro-elastic problem above has been always a great challenging. As pointed out by Kanfa et al.,[6] most studies in the literature assume that the pore pressure is the initial reservoir pressure around the borehole wall to simplify the problem. The effect of pore pressure variation due to the steady flow on the wellbore stability was recently considered by Do et al.[7] An extension of this analytical solution was then conducted in Ref. 8 in which the one-way hydro-mechanical (HM) coupling was adopted by neglecting the mechanical effect (i.e., the second term in brackets in Eq. (6)) on the variation of pore pressure. Following that, the closed-form solution of this last problem was derived by these authors using the well-known complex potential approach introduced by Lekhnitskii.[11] As a function of time, the solution of this uncoupled problem approaches the fully coupled problem and attains the solution of steady state at long term.[19]

The stability of the wellbore immediately after the quick extraction for the low permeable rocks like shale is another important case that the closed-form solution can be derived. This phenomenon is referred to as the "undrained" drilling effect when the change of stresses (i.e., rate of loading) is much faster than the capacity of the rock to dissipate induced excess pore pressure which is calculated as follows[22,39]:

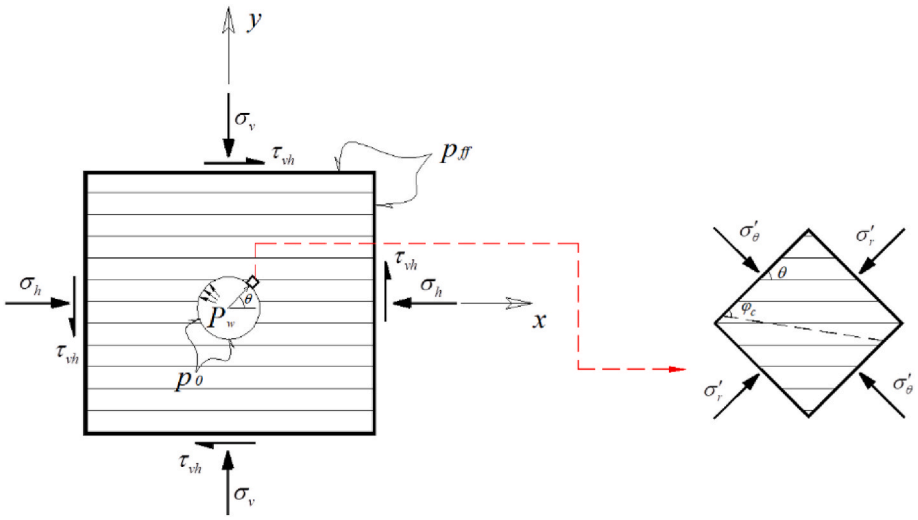

Fig. 2. Critical plane characterized by the inclined angle φ_c at which the shear failure initiates. This critical plane can coincide (i.e., $\varphi_c = \theta$) or have different orientation (i.e., $\varphi_c \neq \theta$) with respect to the weak plane according to the Jaeger model.

$$\Delta p = -\frac{\beta_1\sigma_x + \beta_2\sigma_y}{\beta_3},$$
$$\beta_1 = s_{11}\alpha_x + s_{12}\alpha_y, \quad \beta_2 = s_{12}\alpha_x + s_{22}\alpha_y, \quad \beta_3 = \frac{1}{M} + \alpha_x\beta_1 + \alpha_y\beta_2, \tag{10}$$

In this study, three cases are considered relating to the pore pressure state around the wellbore. The first case adopts the initial uniform pore pressure by ignoring the fluid flow in the rock formation. This case, as usually accepted in the literature, will be noted hereafter as the impermeable boundary problem. The second one, called the permeable boundary problem, considers the effect of steady flow on the mechanical behavior of the wellbore. The last case consists in the undrained problem to consider the stability of the wellbore immediately after drilling.

To simplify the presentation, only the final expressions of the effective radial and tangential stresses on the wall of the wellbore of these cases are summarized in Appendices A and B. For more details about the derivation of these closed-form solutions, the interested readers can refer to Refs. 7,8,19,20,22,39. The effective radial and tangential stresses at a point on the well wall, characterized by an inclination angle θ ($\theta \in [0,\pi]$) with respect to the horizontal axis *Ox* as shown in Fig. 2, depend on the initial pore pressure p_{ff}, the wellbore pressure P_w, the initial far-field stress, as well as the anisotropic poro-elastic properties of the surrounding rock:

$$\sigma'_\theta = f\left(E_x, E_y, \nu_{xy}, \nu_{xz}, G_{xy}, k_x, k_y, \theta, \beta, K_0, \sigma_v^{ff}, \alpha_x, \alpha_y, M, p_0, p_{ff}, P_w\right),$$
$$\sigma'_r = -P_w + \left(\alpha_x.\cos^2\theta + \alpha_y.\sin^2\theta\right)p_0, \tag{11}$$

with the pore pressure on the well wall $p_0 = P_w$ for the case of permeable boundary, $p_0 = p_{ff}$ for the case of impermeable boundary, or $p_0 = p_{ff} + \Delta p$ for the undrained case.

2.2. Fracture initiation pressure

It has been largely accepted that tensile failure occurs when the effective tangential stress on the well wall exceeds the tensile strength of the massif. Among different models to characterize tensile strength of transversely isotropic rock, the well-known model of Nova and Zaninetti[7,40,41] is chosen in this work to calculate the fracture initiation pressure. According to this model, the tensile strength for an inclined plane, characterized by the angle θ_t ($\theta \in [0,\pi/2]$) between its normal vector $\mathbf{n} = (-\sin\theta_t, \cos\theta_t, 0)$ with respect to the normal vector of the bedding plane, is defined as:

$$T(\theta_t) = \frac{T_{90} + T_0}{2} - \frac{T_{90} - T_0}{2}\cos 2\theta_t = \frac{(k_T + 1)T_0}{2} - \frac{(k_T - 1)T_0}{2}\cos 2\theta_t, \tag{12}$$

where T_0 and T_{90} are respectively the tensile strengths of the plane parallel and perpendicular to the bedding plane; and $k_T = T_{90}/T_0$ represents the anisotropic degree of the tensile strength for the transversely isotropic medium. Note that, the inclination angle θ_t relates to θ as follows:

$$\theta_t = \begin{cases} \theta & \text{if} \quad \theta \in [0, \pi/2] \\ \pi - \theta & if \quad \theta \in [\pi/2, \pi] \end{cases} \tag{13}$$

The combination of Eqs. 11 and 12 yields the expression of the fracture initiation pressure $P_{w\theta}^{ini}$ at a point characterized by an angle θ on the wellbore wall:

$$\sigma'_\theta\left(E_x, E_y, \nu_{xy}, \nu_{xz}, G_{xy}, k_x, k_y, \theta, \beta, K_0, \sigma_v^{ff}, \alpha_x, \alpha_y, M, p_{ff}, P_w\right) = T(\theta), \tag{14}$$

Due to the dependence of the effective tangential stress on anisotropic poro-elastic properties, the anisotropic tensile strength of the rock, the initial far-field stresses, and the orientation of the bedding plane, the solution of tensile pressure $P_{w\theta}^{fra}$ at each inclined plane θ depends also on these parameters and can be expressed in the following form:

$$P_{w\theta}^{fra}(\theta) = g\left(E_x, E_y, \nu_{xy}, \nu_{xz}, G_{xy}, k_x, k_y, \theta, \beta, K_0, \sigma_v^{ff}, \alpha_x, \alpha_y, M, p_{ff}, k_T, T_0\right), \tag{15}$$

The fracture initiation pressure is then determined as the minimum value of $P_{w\theta}^{fra}(\theta)$ with $\theta \in [0, \pi]$:

$$P_w^{fra} = \underset{\theta\in[0,\pi]}{\text{Min}}\left[P_{w\theta}^{fra}(\theta)\right] = \left[P_{w\theta}^{fra}(\theta_c)\right] \tag{16}$$

where the critical plane characterized by θ_c at which the fracturing initiates is determined from the following equation:

$$\left.\frac{\partial P_{w\theta}^{fra}(\theta)}{\partial\theta}\right|_{\theta=\theta_c} = 0 \tag{17}$$

2.3. Collapse pressure

The instability of the wellbore due to collapse occurs when the surrounding stress state exceeds the shear strength of the rock formation. Thus, the determination of collapse pressure depends strongly on the chosen criterion of shear failure.

Research on the shear failure of anisotropic rock remains an active topic despite numerous contributions in the literature. Several sophisticated models have been developed to reproduce the laboratory and in-situ observation.[4,41–47] However, their application in practical petroleum engineering seems limited because of their high number of associated parameters whose physical meaning and calibration are not simple to be evaluated.

In the present paper, the model of Jaeger[42,46] is chosen to evaluate the collapse pressure. As a reminder, Jaeger[42] used the Mohr-Coulomb failure criterion to define the shear strength of the rock mass having a set of parallel planes of weakness. Also known as the single weakness plane theory, this model supposes that failure can take place in the weak plane characterized by its shear strength or in the other planes characterized by the strength of the intact rock. So far, the application of the Jeager model has been largely used and discussed in the literature. For example, in Ref. 5, the author showed that the shear failure in a sample under the compressive test can occur in the plane of weakness if the inclination angle θ (i.e. angle between the direction of the maximum compressive stress and the normal of the plane of weakness) varies from the friction angle of the plane of weakness φ_w to 90°. Outside this range, the orientation of the failure plane (i.e. the critical plane φ_c) can be different from that of the weakness plane and is controlled by the strength of intact matrix rock (see Fig. 2). From the triaxial compressive tests performed on a shale rock, the authors in Ref. 17 observed the 'U-shaped' of curve between compressive strength with respect to the inclination angle θ. The minimum value of strength is found at 55° while the strength is maximum at θ = 0° and 90°. This 'U-shaped' is also remarked in the previous contribution of Aadnoy et al.[16] Application in the context of stability of inclined wellbore and under the three-dimensional stress state, these last authors reveal the conditions where the plane of weakness control wellbore failure. Following that, the wellbore failure at the plane of weakness depends not only on the shear strength of the bedding plane but also on the combinations of borehole orientation and magnitude of the in-situ stresses. Always in the condition of three-dimensional stress state of inclined wellbore, Setiawan and Zimmerman[14] used the Mogi-Coulomb and Jeager models to describe the failure criteria of intact rock and the bedding plane. In addition to the high effect of plane of weakness, they also demonstrated the important role of the intermediate stress on the stability of wellbore. In comparison with this last contribution and for the sake of clarity, we note here that the Mohr-Coulomb model is also chosen as failure criterion of intact rock regarding with our plane strain assumption for the considered horizontal wellbore.

Mathematically, the shear failure of intact rock is described by two well-known parameters: the cohesion C_i and friction angle φ_i according to the Mohr-Coulomb model:

$$\frac{\left(\sigma_r^{'}-\sigma_\theta^{'}\right)}{2}+\frac{\left(\sigma_r^{'}+\sigma_\theta^{'}\right)\sin(\varphi_i)}{2}-C_i\cos(\varphi_i)=0 \tag{18}$$

In Eq. (18), the two major and minor principal stresses are directly replaced by the effective radial and tangential stresses and the compressive stress is negative as assumed previously.

Correspondingly, the shear failure at the weak plane, characterized by the inclined angle $\theta_w \in [0, \pi/2]$, depends on the cohesion C_w and the friction angle φ_w which are lower than the ones of the intact rock (i.e., $C_w < C_i$, $\tan(\varphi_w) < \tan(\varphi_i)$):

$$\frac{\left(\sigma_r^{'}-\sigma_\theta^{'}\right)\sin(2\theta_w)}{2}=C_w-\left(\sigma_r^{'}.\sin(\theta_w)^2+\sigma_\theta^{'}.\cos(\theta_w)^2\right)\tan(\varphi_w) \tag{19}$$

with

$$\theta_w=\begin{cases}\theta & \text{if} \quad \theta\in[0,\pi/2]\\ \pi-\theta & if \quad \theta\in[\pi/2,\pi]\end{cases} \tag{20}$$

From Eqs. 18 and 19, we can deduce the following collapse pressure $P_{w\theta}^{col}$ with respect to θ (with $\theta \in [0, \pi]$):

$$P_{w\theta}^{col}(\theta)=\mathrm{Max}\left(P_{w\theta}^{\mathrm{int}}(\theta),P_{w\theta}^{wp}(\theta)\right) \tag{21}$$

where $P_{w\theta}^{wp}(\theta)$, $P_{w\theta}^{\mathrm{int}}(\theta)$ are the collapse pressure corresponding to the shear failure of the bedding plane and of intact rock.

Finally, the collapse pressure that ensures the stability of wellbore from shear failure is evaluated from the maximum value of $P_{w\theta}^{col}(\theta)$ calculated from Eq. (21) with $\theta \in [0, \pi]$:

$$P_w^{col}=\underset{\theta\in[0,\pi]}{\mathrm{Max}}\left(P_{w\theta}^{col}(\theta)\right) \tag{22}$$

3. Safe mud pressure window of horizontal wellbore in anisotropic rock

The heterogeneous characteristic in nature of rock mass, as well as the deficiencies in human knowledge due to the limitation or lack of test data, are considered as the principal uncertainty sources of input parameters in rock engineering design. In petroleum-related applications, logs data are widely used to calibrate the input parameters against core data. The logs data involve different sources of uncertainty related to the malfunctioning of the device and human error during acquisition and interpretation. This paper does not intend to discuss the uncertainty of the calibrated input parameters (e.g., the in-situ stress state, pore pressure, the mechanical properties of rock mass) by log-based correlations which were largely pointed out by many previous studies.[2,28,29,33,37,48] It is worth also noting that the characterization of the transversely isotropic rock remains nowadays a challenging issue and the associated uncertainty could be much higher when the anisotropic effect is accounted for.

From the methodology point of view, the traditional wellbore pressure design bases on the deterministic solution, which can highly underestimate the collapse pressure and overestimate the fracture initiation pressure resulting in a large mud weight window.[1,2,38] By using the probabilistic analysis that can consider the uncertainty of input parameters to verify the reliability of the deterministic results, different studies highlighted much narrower safe pressure windows.[26–36,48] Consequently, the consideration of uncertainty through the probabilistic assessment (also called the risk or stochastic analysis) seems extremely necessary for the optimization design of the wellbore. Among various probabilistic analysis methods, the Monte Carlo Simulation (MCS) is the most widely used and can be chosen as the referent approach to validate the other stochastic techniques.[24,25] The main idea of the MCS is to construct the limit state functions (LSF) that separate the safe and failure domains by point-by-point evaluations from the large random samples of input variables. In the present work, this well-known probabilistic analysis method is also chosen to quantify the uncertainty effect on the safe mud pressure window as well as to validate the Kriging metamodeling technique which is firstly adapted to solve the stochastic analysis of wellbore.

3.1. Deterministic results

Before performing the sensitivity and probabilistic analysis, we discuss firstly the results of the deterministic problem. For this purpose, the stability of the horizontal wellbore drilled in a VTI rock like Tournemire shale at a depth of 1000 m is considered. The transversely poroelastic properties of this argillaceous rock are taken in the previous studies[49–53] whilst their corresponding anisotropic tensile and shear strengths are extracted from .[45] Table 1 summaries the adopted hydro-mechanical properties of this shale rock, as well as the stress state and pore pressure at the far-field. In addition, due to the lack of the statistical data, these parameters are considered as the mean values while the same coefficient of variation COV = 30% is assumed in this work to characterize the uncertainty of these input parameters. For the sensitivity analysis and then for the stochastic analysis in the next parts, the normal distribution of each input parameter A is truncated at 95%

Table 1
In-situ stress state, pore pressure and mechanical properties of the transversely isotropic Tournemire shale.

Initial stress state and pore pressure				Poro-elastic properties			
Parameter	Mean	Min	Max	Parameter	Mean	Min	Max
σ_v^{ff} (MPa)	-26.5	-10.92	-42.08	E_x (GPa)	27.93	11.51	44.35
$K_0 = \sigma_h^{ff}/\sigma_v^{ff}$	1.05	0.43	1.67	$k_E = E_y/E_x$	0.33	0.14	0.52
p_{ff} (MPa)	10	4.12	15.88	G_{xy} (GPa)	3.9	1.61	6.19
β (°)	10	4.12	15.88	α_x	0.17	0.07	0.27
Tensile and shear strengths				M (GPa)	17.14	7.06	27.22
T_0 (MPa)	8	3.30	12.70	k_y/k_x	0.5	0.21	0.79
k_T	2.17	1	3.45	k_x (10^{-13} m/s)	5.5	2.27	8.73
C_w (MPa)	10.88	4.48	17.28	ν_{xz}	0.17	0.07	0.27
φ_w (°)	19.36	7.98	30.74	ν_{yx}	0.2	0.08	0.32
C_i/C_w	1.65	1	2.62				
φ_i/φ_w	1.24	1	1.97				

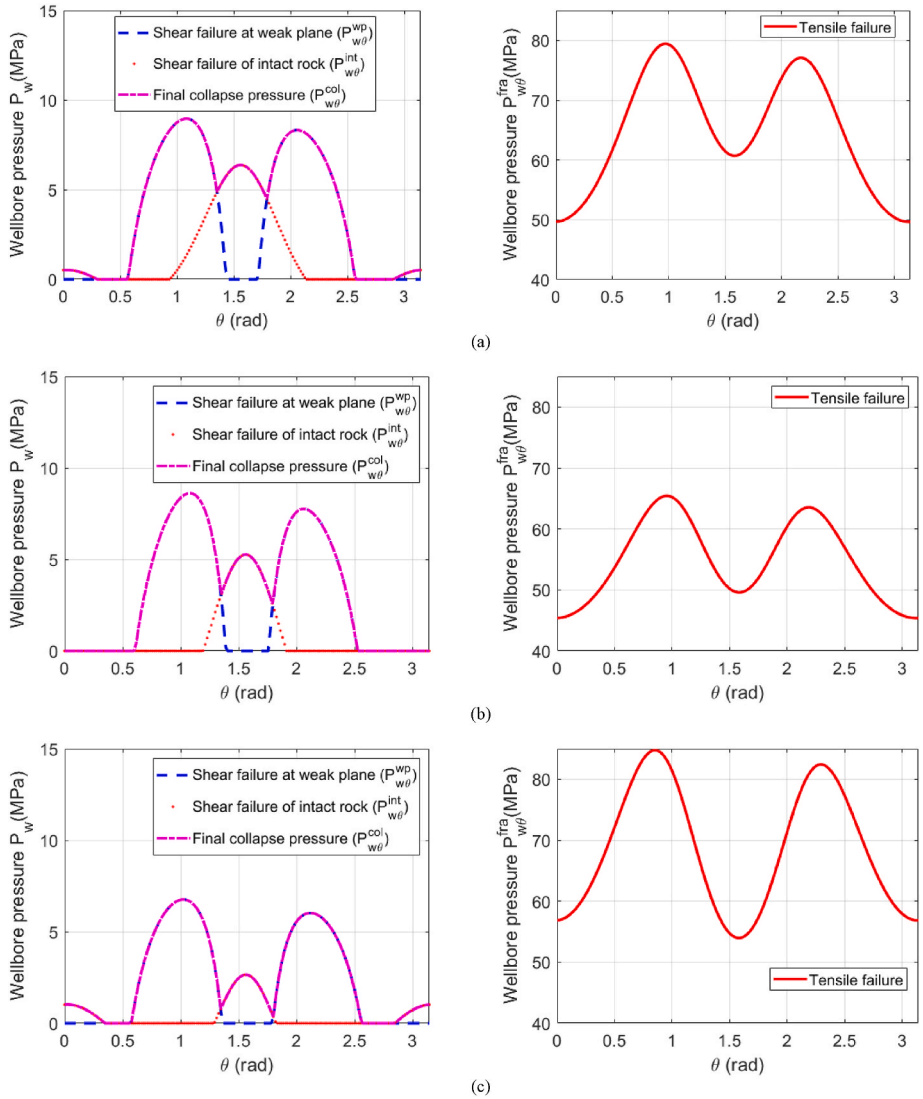

Fig. 3. Evolution of collapse pressures $P_{w\theta}^{col}(\theta)$ and fracture pressure $P_{w\theta}^{fra}(\theta)$ versus inclination angle θ in the case: impermeable boundary (a), permeable boundary (b) and undrained problem (c).

confidence interval thus the corresponding minimum and maximum values (A_{min} = (1-1.96COV). A_{mean} and A_{max} = (1 + 1.96COV). A_{mean}) can be calculated and are also detailed in Table 1.

Fig. 3 presents the deterministic solution of collapse and fracture pressures versus the inclination angle θ (θ∈[0,π]) for three considered cases of the horizontal well (i.e., impermeable boundary, permeable boundary, and undrained cases). The results calculated from the mean value of input parameters show that the anisotropic behavior of shale rock and the adopted state of pore pressure around the well wall can significantly affect the distribution of fracture and collapse pressures in

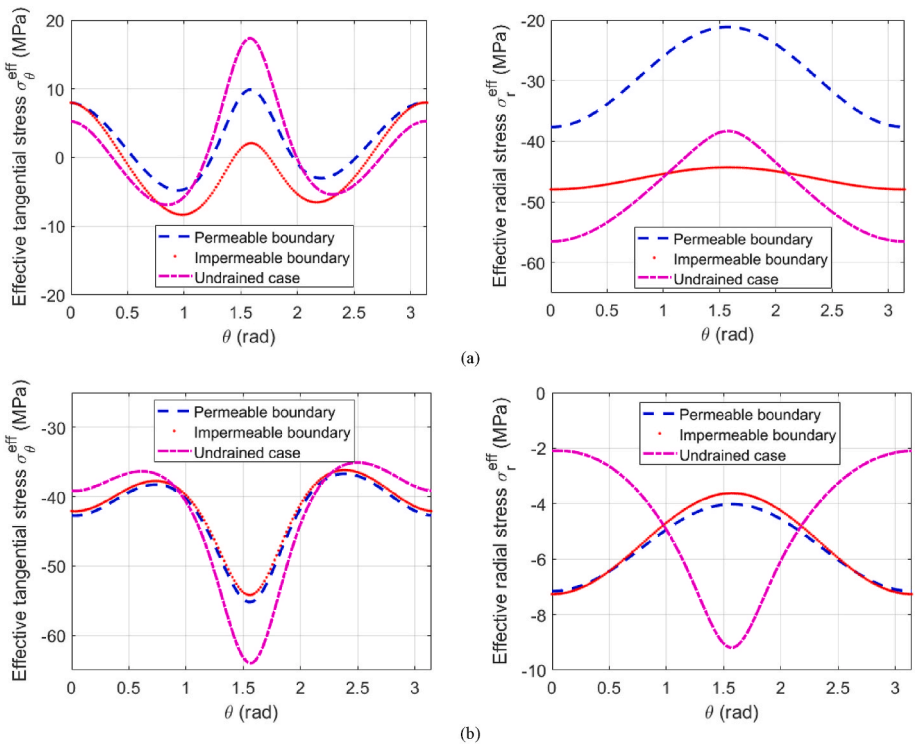

Fig. 4. Distribution of effective tangential and radial stresses on the well wall using fracture pressure P_w^{fra} (a) and collapse pressure P_w^{col} (b) in the wellbore.

the wellbore. For the case of uniform initial pore pressure by neglecting the effect of hydro-mechanical coupling, the values of 8.99 MPa and 49.65 MPa can be noted as the safe mud pressure window corresponding to the shear and tensile failure of the horizontal wellbore. Those values are respectively equal to 8.66 MPa and 45.37 MPa in the case of a permeable boundary at the well wall (i.e., case of steady fluid flow) whilst the mud pressure in the range of 6.76 MPa–53.96 MPa ensures the stability of the wellbore immediately after drilling by adopting the undrained condition. Thus, these deterministic results highlight that the mud pressure window is largest in the undrained case representing by the lowest collapse pressure and highest fracture pressure. The comparison between the impermeable and permeable boundary conditions at the well wall shows that both the collapse and fracture pressures in the wellbore are higher in the former case and the difference seems more pronounced on the fracture pressure than the collapse pressure. This can be explained by the high contrast between the fracture pressure in the wellbore and the initial pore pressure of rock mass that induces a significant variation of stress state on the circumference of horizontal well.

Fig. 4 highlights the distributions of effective stress state on the wall of the wellbore corresponding to the fracture initiation pressure P_w^{fra} and the collapse pressure P_w^{col} in cases of impermeable and permeable boundary conditions, as well as the undrained problem. For the two former cases, the results of stress state at the shear failure are quite similar (Fig. 4a) but their difference becomes much stronger for the tensile failure state (Fig. 4b). This can be explained by the fact that the higher wellbore pressure increases the compressive radial stress but decreases the compressive tangential stress on the well wall. Furthers, this variation is much more pronounced in the permeable boundary condition especially at the horizontal and vertical planes (e.g., $\theta = 0$ and $\theta = \pi/2$) of the wellbore. Although in both cases of impermeable and permeable boundary conditions, a fracture can initiate at the horizontal plane ($\theta = 0$), we can note however that the maximum tensile stress in the permeable rock is located at $\theta = \pi/2$ whose value is however still lower than the tensile strength of this vertical plane. The results of this deterministic problem confirm the important effect of anisotropy and the interaction of different input parameters on the distribution of stress state and failure of the wellbore as demonstrated in Refs. 7,8. Regarding the results of the undrained case, we can observe a similar tendency of

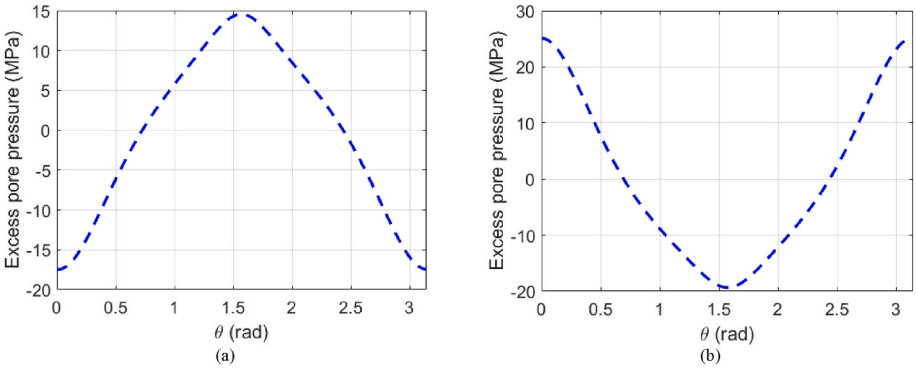

Fig. 5. Distribution of excess pore pressure on the well wall in the undrained case using fracture pressure P_w^{fra} (a) and collapse pressure P_w^{col} (b) in the wellbore.

Table 2
Mechanical properties of the isotropic rock using the ones of the vertical direction of the Tournemire shale.

Parameters	E (GPa)	ν	α	M (GPa)	k (10^{-13} m/s)	T (MPa)	C (MPa)	φ (°)
Mean	9.22	0.2	0.53	17.14	2.75	8	10.88	19.36
Min	3.80	0.08	0.22	7.06	1.13	3.30	4.48	7.98
Max	14.64	0.32	0.84	27.22	4.37	12.79	17.28	30.74

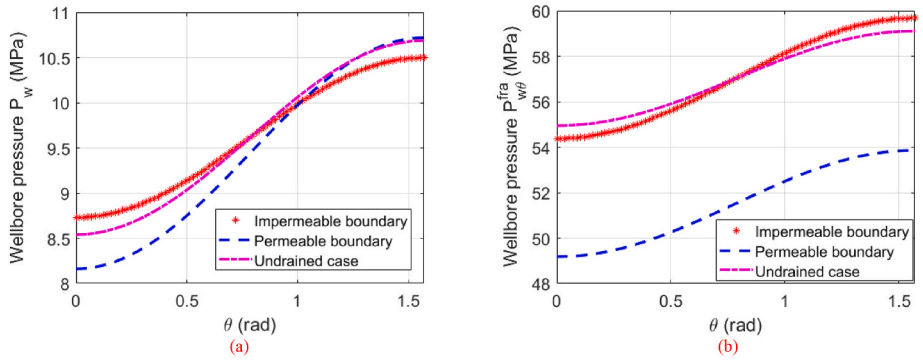

Fig. 6. Evolution of collapse pressures $P_{w\theta}^{col}(\theta)$ and fracture pressure $P_{w\theta}^{fra}(\theta)$ versus inclination angle θ in the case: impermeable boundary (a), permeable boundary (b) and undrained problem (c) of the isotropic rock.

stress distribution as the two previous cases using the fracture pressure in the wellbore. However, the maximum tensile strength located at $\theta = \pi/2$ exceeds the tensile strength in this undrained case which induces the tensile failure in the vertical plane instead of the horizontal plane as depicted in Fig. 3c. The difference of the undrained response of the wellbore in comparison with the impermeable and permeable boundary conditions is clearer when the collapse pressure is taken in the wellbore. Follow that, the non-uniform excess pore pressure in the undrained case (Fig. 5) can significantly affect the distribution of effective stresses on the well wall when the maximum compressive stress is located at the vertical plane $\theta = \pi/2$ for both the radial and tangential stresses.

Now we compare these deterministic results of collapse and fracture pressures of anisotropic rock with the ones calculated for the isotropic rock. For this purpose, the mechanical properties extracted from the vertical direction of the Tournemire shale are chosen for the isotropic rock. Following that, the Young's modulus and Poisson ratio of the isotropic rock are chosen $E = E_y$, $\nu = \nu_{yx}$ whilst its corresponding parameters characterize the tensile and shear strengths are equal to the ones of the bedding plane of the anisotropic rock (see Table 2). Note that, for the sake of clarity, the classical expressions of stress state and

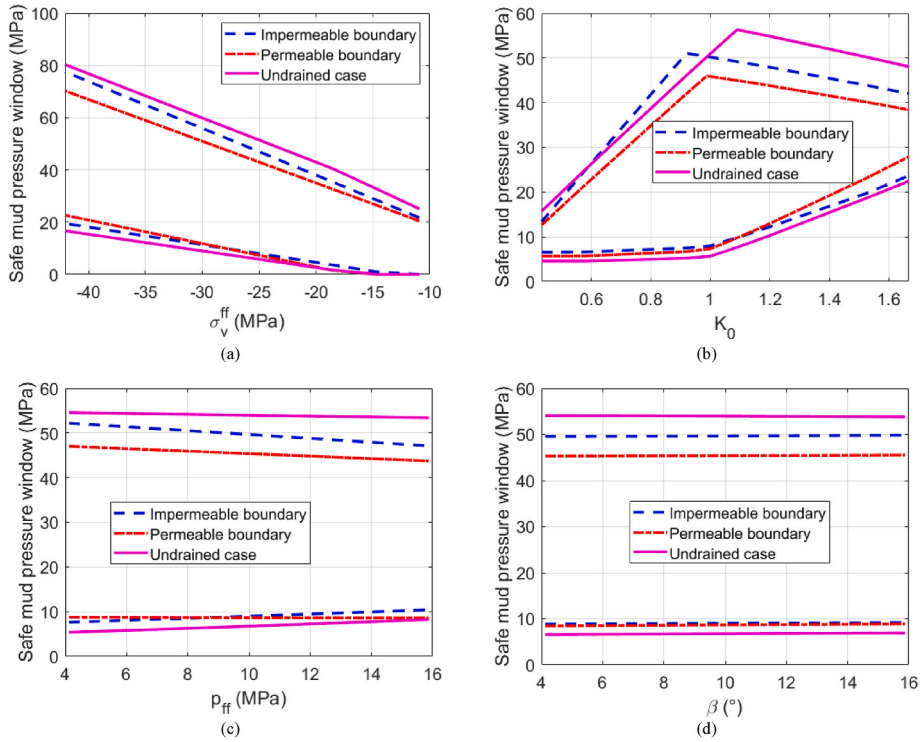

Fig. 7. Effect of vertical initial stress σ_v^{ff} (a), initial stress ratio K_0 (b), initial pore pressure p_{ff} (c) and inclination angle β (d) on the safe mud pressure window of wellbore in the impermeable boundary, permeable boundary, and undrained cases.

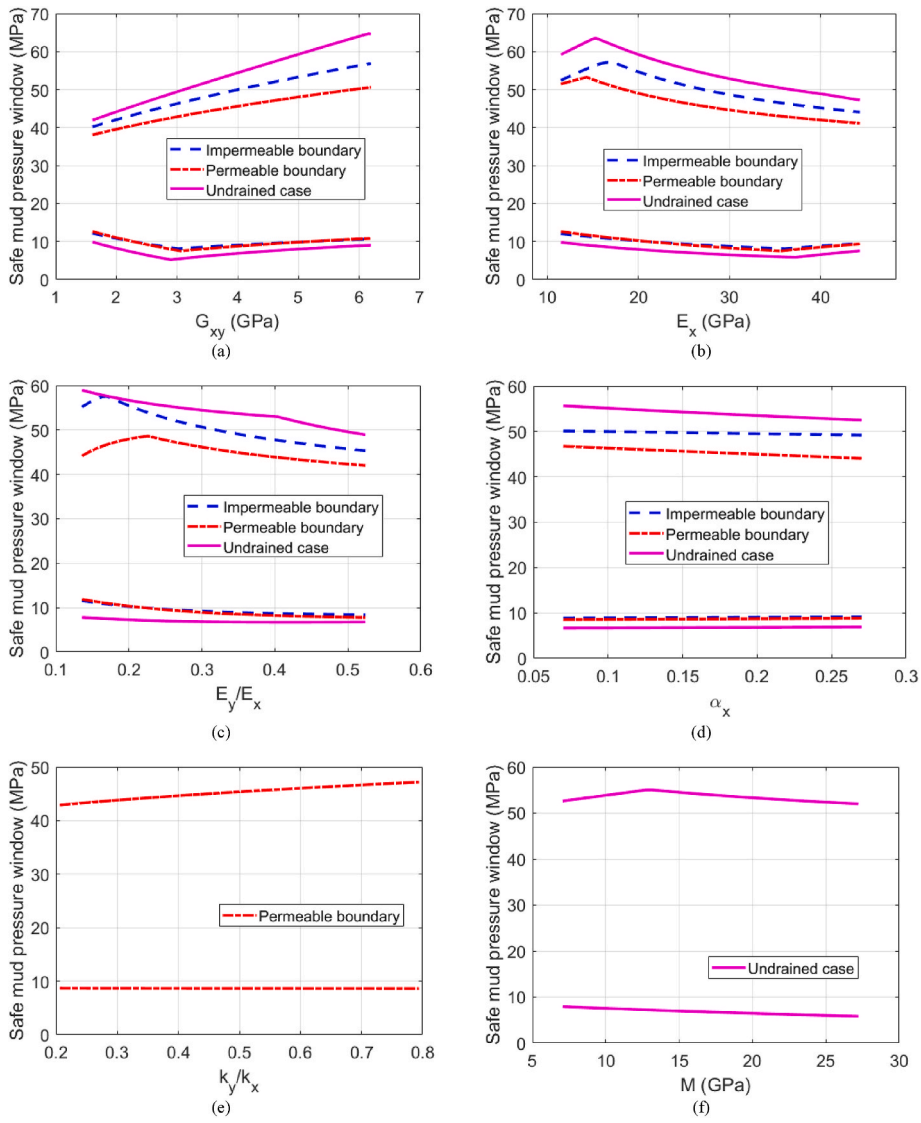

Fig. 8. Effect of shear modulus G_{xy} (a), Youngs's modulus E_x (b), Young's modulus ratio E_y/E_x (c), coefficient of Biot α_x (d), permeability ratio k_y/k_x (e) and Biot modulus M (f) on the safe mud pressure window of wellbore in the impermeable boundary, permeable boundary, and undrained cases.

pressures at failure of wellbore drilled in the isotropic rock and under different conditions of impermeable and permeable boundaries as well as undrained behavior are summarized in Appendix C.

Fig. 6 illustrates the evolution of collapse and fracture pressures of the wellbore drilled in this isotropic rock. Due to the higher compressive stress in the horizontal direction at far-field, the highest collapse pressure is found at $\theta = \pi/2$ whilst lowest fracture pressure is at $\theta = 0$ for all three cases of impermeable, permeable boundaries and undrained rock. Like the anisotropic rock, these results reveal that the permeable boundary case presents the narrowest safe mud pressure window which ranges from 10.72 MPa to 49.18 MPa. However, both these last values are higher than the ones calculated from the anisotropic rock.

3.2. Sensitivity analysis

The sensitivity analysis is undertaken in this part to determine the role of each parameter on the variation of the safe pressure window of wellbore in the anisotropic rock. The sensitivity analysis is essential since it helps the experimental campaign to put more effort into the parameters significantly affecting the safe pressure window variation. For this purpose, the mono-parametric investigation is conducted by considering only the variation of each considered parameter whilst all the other properties are fixed.

To simplify the presentation, only the results of the key parameters such as the initial stress state, pore pressure (Fig. 7), poro-elastic properties (Fig. 8), and strength properties (Fig. 9) of rocks are shown. The first remark is made on the important effect of the initial stress state on the variation of collapse and fracture pressures. By varying the value of the initial vertical stress σ_v^{ff} or the anisotropic coefficient K_0, the mud pressure window changes considerably. Follow that, the decrease of σ_v^{ff} induces a strong decrease of both collapse and fracture pressures in the horizontal wellbore (Fig. 7a). The increase of K_0 reveals an increase of collapse pressure in the wellbore whilst the fracture pressure can become smaller at the high degree of anisotropy of the initial stress state (Fig. 7b). However, it seems that the variation of pore pressure in the rock mass affects quite slightly the evolution of mud pressure window (Fig. 7c) while the variation of the inclination angle of bedding plane β in the range of [4.12°, 15.88°] does not affect the safe mud pressure window in all cases (Fig. 7d).

Among different poro-elastic properties of the transversely isotropic rocks, the influence of shear modulus G_{xy}, horizontal Young' modulus E_x and the ratio E_y/E_x are the most pronounced (Fig. 8). A higher value of shear modulus G_{xy} results in higher fracture pressures (Fig. 8a).

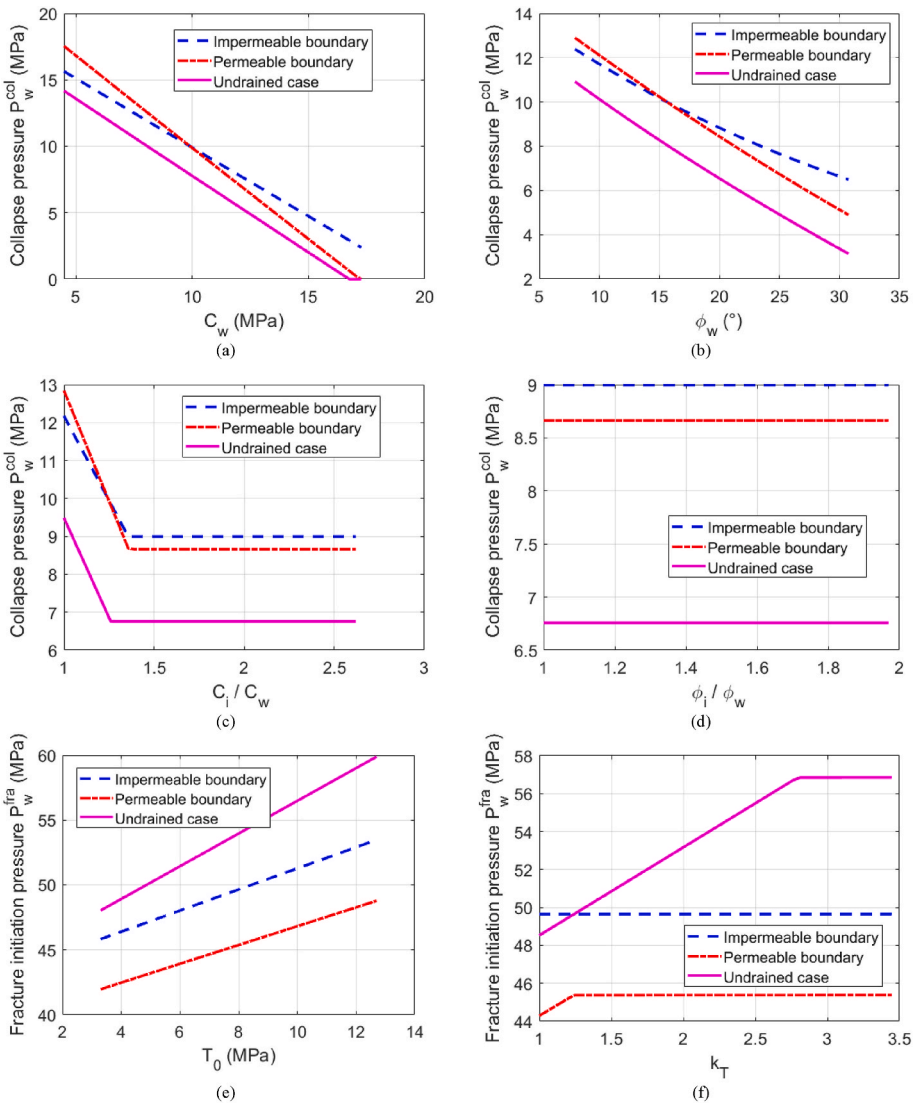

Fig. 9. Effect of shear strength parameters like cohesion C_w (a), friction angle of the weak plane φ_w (b), cohesion's ratio C_i/C_w (c), friction angle ratio φ_i/φ_w (d) on the collapse pressure and tensile strength T_0 (e), k_T (f) on the fracture initiation pressure of wellbore in the impermeable boundary, permeable boundary, and undrained cases.

Inversely, an increase of Young's modulus in the horizontal or vertical direction (represented by a higher value of E_y/E_x) reduces the safe mud pressures in the wellbore (Fig. 8b and c). By varying the Biot coefficient in the range $\alpha_x \in [0.17, 0.27]$, its effect on the wellbore pressures seems moderate in all cases of impermeable and permeable boundary conditions, as well as the undrained problem (Fig. 8d). The same remark can be noted for the permeability's ratio k_y/k_x (or the Biot modulus M) when the higher value of this parameter can increase slightly the fracture pressure of wellbore in the permeable boundary (or undrained case) as illustrated in Fig. 8e and f.

Regarding the strength properties of shale rock, the cohesion of the weak plane C_w affects the most the variation of collapse pressure in the wellbore (Fig. 9a). The decrease of this last pressure is remarkable when the value C_w attains its maximum value. In comparison with the cohesion, the influence of friction angle of the weakness plane φ_w is smaller (Fig. 9b). The anisotropic effect of shear strength is characterized by the two ratios C_i/C_w and φ_i/φ_w. The results exhibited in Fig. 9c show that a ratio of C_i/C_w approaches to 1 can significantly increase the collapse pressure in the wellbore. In this case, the shear failure on the well wall does not occur at the plane of weakness but at the vertical plane of the intact rock ($\theta = \pi/2$). The other ratio φ_i/φ_w does not present any effect on the mud pressure window of the wellbore (Fig. 9d). Concerning the effect of tensile properties of the Tournemire shale, we observe that the tensile strength of the horizontal plane T_0 presents its considerable effect on the variation of fracture pressure in all considered cases of the wellbore (Fig. 9e). The influence of the anisotropic tensile strength characterized by the parameter k_T seems slight in the impermeable and permeable boundary conditions but significant in the undrained case (Fig. 9f).

The results of the sensitivity analysis can also be represented in the well-known Tornardo chart for parameter ranking (Figs. 10 and 11). From these diagrams, one can conclude that the initial stress state characterized by the vertical stress σ_v^{ff} and the anisotropic coefficient K_0 is the most sensitive parameters on the safe mud pressure windows of the horizontal well drilled in the Tournemire shale. Indeed, the variation of σ_v^{ff} results in a wide range of fracture and collapse pressures representing a strong variation of the safe mud weight window. It indicates that the influence of the shear strength of the weak plane (e.g., C_w, φ_w) on the collapse pressure is higher than the ones of the anisotropic elastic properties (e.g., G_{xy}, E_x, E_y/E_x). In turn, these later parameters have more effect on the fracture initiation pressure than the tensile strength parameters (T_0, k_T). The role of the pore pressure and coefficient of Biot

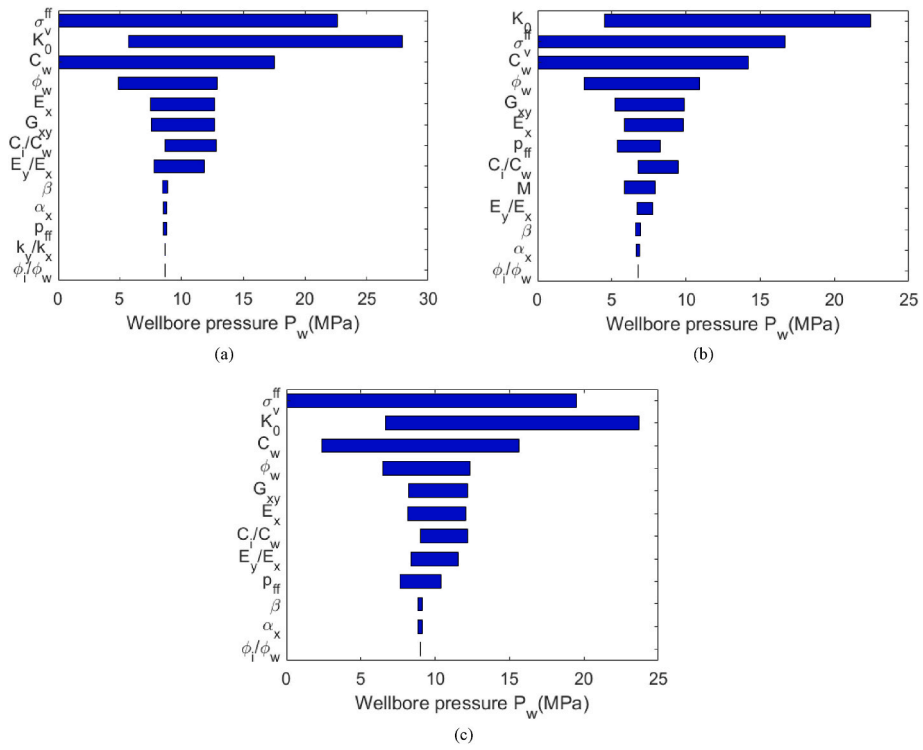

Fig. 10. Sensitivity analysis of collapse pressure in wellbore exhibited in tornardo graph: permeable boundary (a), undrained problem (b) and impermeable boundary (c).

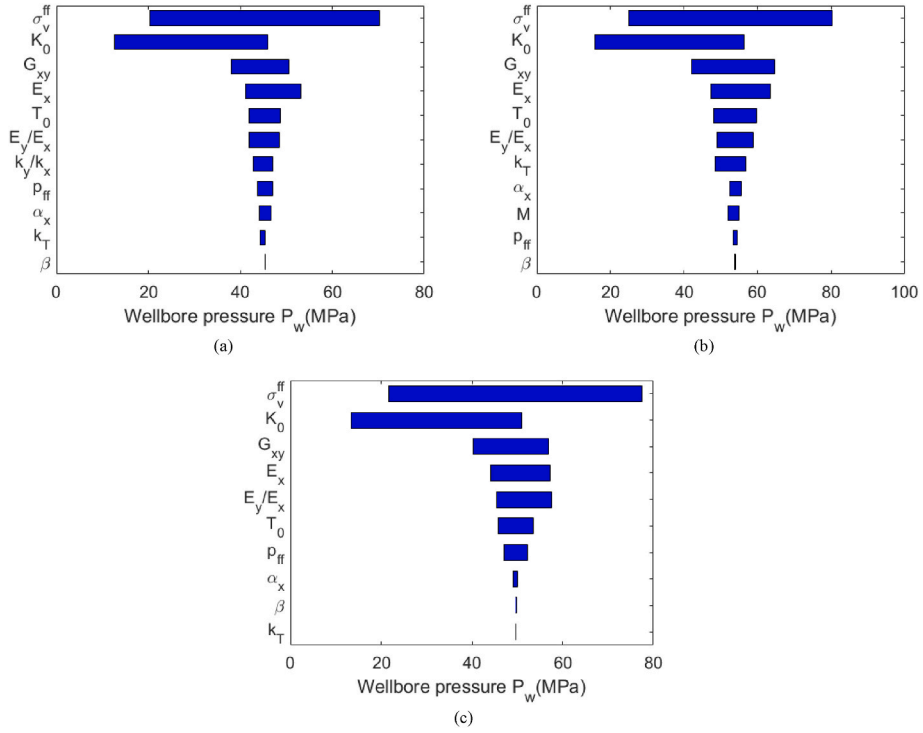

Fig. 11. Sensitivity analysis of fracture initiation pressure in wellbore exhibited in tornado graph: permeable boundary (a), undrained problem (b) and impermeable boundary (c).

α_x on the results of safe mud weight window is moderate. It is also the case of the permeable ratio k_y/k_x and Biot modulus M when they can impact slightly on the variation of the fracture pressure in the permeable boundary and undrained cases. From the results of this sensitivity study, it indicates that the effects of the other parameters like the inclination angle of bedding plane β, and the ratio of friction angle φ_i/φ_w are negligible and can be omitted in the stochastic assessment for the horizontal wellbore drilled in Tournemire shale. The sensitivity analysis performed in this work allows us to confirm and extend the conclusion of various works in the literature, which however are mainly limited in the

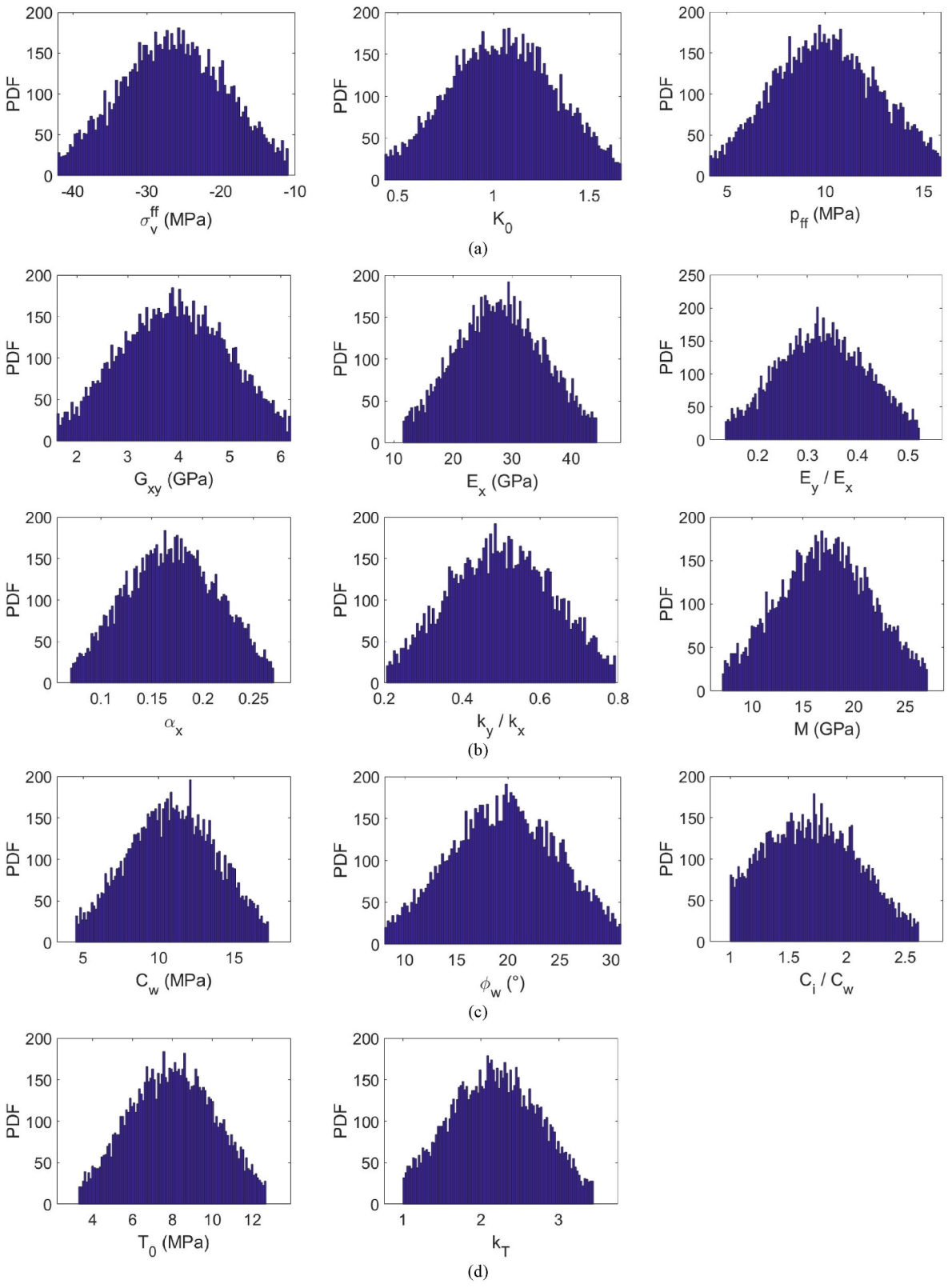

Fig. 12. Probability distribution function (PDF) of ten thousand randomly generated samples used in the MCS: initial stress state and pore pressure (a), poro-elastic properties (b), shear strength parameters (c) and tensile strength properties (d) of Tournemire shale rock.

case of isotropic poro-elastic rocks.[26–34,48]

In general, the deterministic results and the sensitivity analysis conducted in this section show that the safe mud pressure window in the wellbore is largest in the undrained case. Furthermore, in comparison with the impermeable boundary case, where the variation of pore pressure around the wellbore is neglected, the mud pressure window seems narrower when the variation of pore pressure due to the steady-state flow is accounted for (i.e., permeable boundary case).

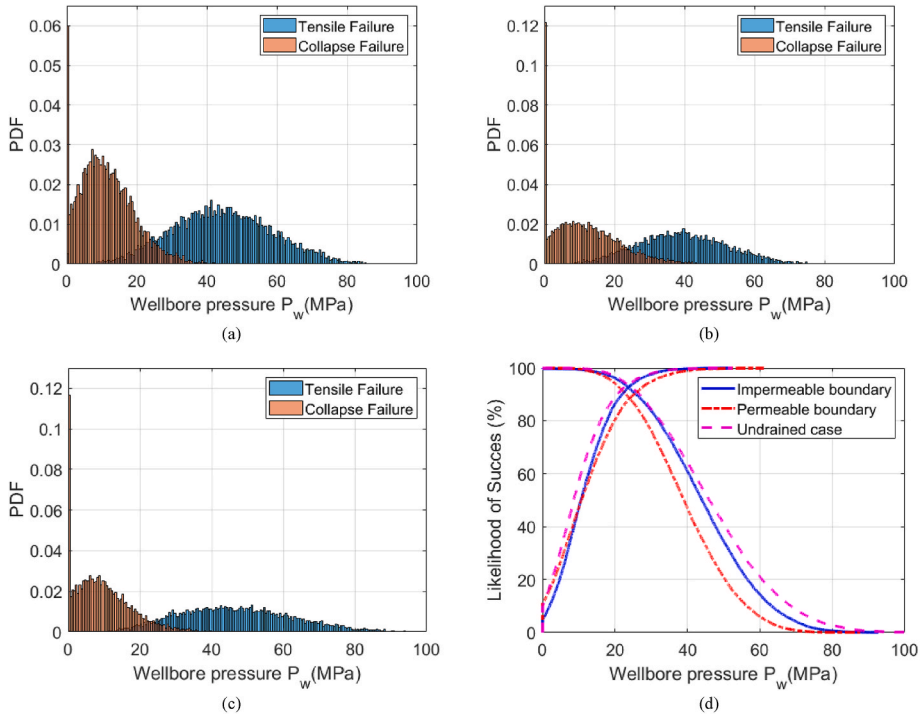

Fig. 13. Probability distribution function (PDF) of wellbore pressure in the impermeable boundary (a), permeable boundary (b), undrained case (c) and their likelihood of success (d).

Table 3
Safe mud pressure windows in the deterministic problem and probabilistic assessment evaluated at confidence level (CL) in the permeable and impermeable boundary and undrained cases.

Case	Permeable boundary		Impermeable boundary		Undrained case	
	P_w^{col} (MPa)	P_w^{fra} (MPa)	P_w^{col} (MPa)	P_w^{fra} (MPa)	P_w^{col} (MPa)	P_w^{fra} (MPa)
Deterministic	8.66	45.37	8.99	49.65	6.76	53.96
CL = 60%	13.41	35.74	12.70	40.35	10.63	41.80
CL = 70%	16.39	32.32	14.93	36.45	13.06	37.46
CL = 80%	19.88	28.46	17.79	31.99	16.04	32.58
CL = 88%	23.71	24.31	20.83	27.40	19.45	28.11

3.3. Quantification of uncertainty effect

In this part, the probabilistic analysis of wellbore stability is carried out by using firstly MCS to quantify the uncertainty effect combined with the anisotropy of input parameters on the safe mud weight windows. Following that, ten thousand samples of each input parameter A are randomly generated in the range $[A_{min}, A_{max}]$ as summarized in Table 1. We remind that this range is truncated at a 95% confidence interval by assuming the same coefficient of variation COV = 30% for all parameters as mentioned above. Note also that the sensitivity analysis in the previous section reveals the insignificant effect of the friction angle ratio φ_i/φ_w and the inclination angle β, thus their variations are not considered in the stochastic analysis. Similarly, the effect of the variability in Poisson's ratio on the stress distribution around the wellbore and the mud pressures is also negligible.[7,8,19] As an illustration, we present in Fig. 12 the histogram of the initial stress state and pore pressure, the poro-elastic and strength properties of the generated samples of Tournemire shale rock.

Using the closed-form solution of the deterministic problem, the MCS allows calculating the safe mud pressure window of each considered case and for each random sample. Fig. 13 depicts the probability distribution function and the cumulative likelihood of success of the mud pressures of the three considered cases (i.e., impermeable and permeable boundary conditions, as well as the undrained behavior case). In addition, for the comparison purpose, Table 3 recapitulates the safe mud pressure windows evaluated from the deterministic problem and stochastic analysis taken at different confidence of levels (CL). By adopting the higher value of CL, the safe window provided by the probabilistic analysis becomes narrower. For example, at CL = 60% the safe mud window of [13.41 MPa, 35.74 MPa] reduces strongly to [23.71 MPa, 24.31 MPa] at CL = 88% in the case of permeable boundary. Especially, an intersection of the probability of success curves obtained from the fracture and collapse stochastic analysis can be observed at CL = 88.44% in this last case, which signifies that the safe mud pressure window is not available.

The comparison of the results calculated from the three considered cases of wellbore shows that the safe mud pressure window is the largest in the undrained case and the narrowest in the permeable case for all values of CL. For instance, at CL = 88%, the possibility to obtain the safe mud pressure calculated as the difference between the fracture and collapse pressures is about 0.6 MPa for the permeable boundary case whilst this value for the impermeable boundary and undrained cases are about 6.59 MPa and 8.66 MPa respectively. The critical confidence of level is also higher in these two latter cases which are about 92.71% for the impermeable boundary case and 93.78% for the undrained one.

Like the deterministic analysis, we also compare these results of the probabilistic analysis with the one estimated by MCS method for the isotropic rock. The corresponding probabilistic distribution function and the cumulative likelihood of success for the three considered cases of this isotropic rock are depicted in Fig. 14. In comparison with the results illustrated in Fig. 13d of the anisotropic rock, the similar tendency of the likelihood of success can be stated for the isotropic rock formation (see Fig. 14d). More precisely, with the increase of CL, the safe mud pressure window decreases with the narrowest corresponds to the case of the permeable boundary of rock. The recapitulated values in Table 4 show a higher collapse and fracture pressures in all three considered cases of the isotropic rock comparing with the ones of anisotropic rock at the same CL. A lower critical confidence of level at about 84% is also observed in

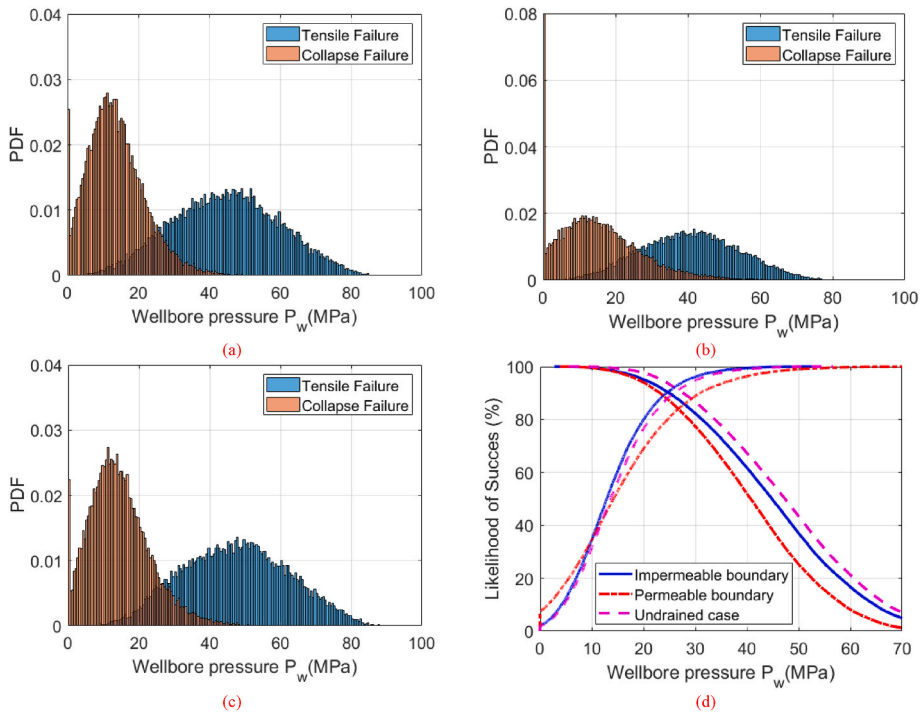

Fig. 14. Probability distribution function (PDF) of wellbore pressure in the impermeable boundary (a), permeable boundary (b), undrained case (c) and their likelihood of success (d) in the isotropic rock.

Table 4
Safe mud pressure windows in the deterministic problem and probabilistic assessment evaluated at confidence level (CL) in the permeable and impermeable boundary and undrained cases of the isotropic rock.

Case	Permeable boundary		Impermeable boundary		Undrained case	
	P_w^{col} (MPa)	P_w^{fra} (MPa)	P_w^{col} (MPa)	P_w^{fra} (MPa)	P_w^{col} (MPa)	P_w^{fra} (MPa)
Deterministic	10.72	49.18	10.49	54.38	10.68	54.94
CL = 60%	17.09	37.10	14.89	40.78	15.72	43.21
CL = 70%	20.36	33.25	17.07	36.32	18.09	38.81
CL = 80%	24.66	28.80	20.02	31.32	21.16	33.82
CL = 84%	26.70	26.73	21.46	29.03	22.71	31.57

the permeable boundary condition of the isotropic. At this critical level, the same value of collapse and fracture pressures (about 26.7 MPa) is higher than the one calculated from the anisotropic rock (about 24 MPa). In general, with respect to the specific considered rock in this work, the difference of safe mud pressure windows of horizontal wellbore drilled in the VTI rock and in the isotropic rock whose properties are extracted from the ones in the vertical direction of the initial anisotropic rock seems moderate. This statement is consistent with the previous sensitivity analysis when the most effect factors on the collapse and fractures pressure in the wellbore are the initial stress state and the strength parameters of the bedding plane.

The strong difference of safe mud pressure windows calculated from the deterministic and stochastic analysis elucidates the crucial role of uncertainty on the wellbore design. It is important to note here that, due to the limit of the analytical approach, the effect of anisotropic hydro-mechanical (HM) coupling on the safe mud pressure window was only considered at short term (i.e., undrained behavior of wellbore immediately after drilling) and at long term (i.e., at steady state regime of fluid flow) whilst the fully HM coupling in the transient state remains a grand challenge. However, thanks to these closed-form solutions, the computational expensive MCS method can be conducted and their results can be used as the reference to investigate the performance of the other techniques in the stochastic analysis of wellbore in the complex contexts (e.g. the fully HM coupling problem, the consideration of thermal and/or chemical effect in anisotropic rocks) that the analytical solutions are no longer available. As an example, in the recent contribution of Do et al.,[24] the Kriging metamodeling technique was successfully adopted to study the failure probability at long term of underground structure constructed in a viscoelastic rock. The efficiency of this metamodel was demonstrated by comparing with the referent results provided by MCS. An extension of Kriging surrogate was then presented in Ref. 25 to assess the probabilistic behavior of a deep drift excavated in the visco-plastic rock in which the deterministic problem must be solved by the numerical simulation.

If the performance of the Kriging metamodel has been revealed in the purely mechanical problem as mentioned above, its applicability to treat the coupling problem in rock mechanical engineering has not yet discussed in the literature. Thus, an adaptation of this metamodeling technique to assess the probabilistic results of safe mud pressure window of the horizontal wellbore drilled in the anisotropic saturated rock, even in the simple case of one-way HM coupling, is extremely useful for the future applications.

As detailed in Refs. 24,25, the principal idea of Kriging metamodel consists of approximating each limit state function (LSF) $G(\mathbf{X})$ that separates the safety ($G(\mathbf{X}) > 0$) and failure domains ($G(\mathbf{X}) \leq 0$) in the space of random input variables gathered in the vector $\mathbf{X}$ by a Gaussian process:

$$G(\mathrm{X}) \approx \overline{G}(\mathrm{X}) = \mathrm{k}(\mathrm{X})^T \beta + Z(\mathrm{X}) \tag{23}$$

The first term $\mathbf{k}(\mathbf{X})^{\mathrm{T}}\boldsymbol{\beta}$ of the Kriging metamodel $\overline{G}(\mathrm{X})$ represents the mean value whilst the second term $Z(\mathbf{X})$ is assumed to have the zero-mean stationary Gaussian process. This metamodel can be built iteratively by determining the unknown parameters $\boldsymbol{\beta}, \sigma_Z^2, \boldsymbol{\theta}$ in which σ_Z^2 is the constant process variance and $\boldsymbol{\theta}$ is the hyperparameter vector of the kernel function $R(\boldsymbol{\theta}, \mathbf{X}, \mathbf{X}')$. To this end, an optimization process is carried out using the exact results of the performance function $G(\mathrm{X})$ at different training points of the Design of Experiment (DoE). This DoE, generated from the Latin Hypercube Sampling (LHS) technique at the

initial step, will be iteratively updated by adding the new training points thank for using a so-called learning function. The procedure will be repeated until the stopping criterion (the convergence) is verified. The interested reader can refer to Refs. 24,25 for more details.

The constructed Kriging metamodel $\overline{G}(\mathrm{X})$ is then used as the predictor to calculate the results of LSF at each random realization of $\mathbf{X}$ through which the MCS can be applied to calculate the failure probability:

$$P_f \approx \frac{1}{N_{MCS}} \sum_{i=1}^{N_{MCS}} \mathbf{I}\left(\overline{G}\left(\mathrm{X}^{(i)}\right)\right), \quad \mathbf{I}\left(\overline{G}\left(\mathrm{X}^{(i)}\right)\right) = \begin{cases} 1 & if \quad \mu_{\overline{G}}\left(\mathrm{X}^{(i)}\right) \le 0 \\ 0 & if \quad \mu_{\overline{G}}\left(\mathrm{X}^{(i)}\right) > 0 \end{cases} \tag{24}$$

where:

$$\mu_{\overline{G}}(\mathrm{X}) = \mathrm{k}(\mathrm{X})^T\overline{\beta} + \mathrm{r}(\mathrm{X})^T\mathbf{R}^{-1}(\mathrm{y} - \mathbf{K}\overline{\beta}) \tag{25}$$

For the concerned problem of wellbore stability in the anisotropic rock, before the application of the Kriging metamodeling technique to determine the safe mud pressure window, two LSF corresponding to the two failure modes (i.e., tensile and shear failures) must be defined. From Eq. (14) that characterizes the tensile failure of wellbore, one can propose the first LSF as follows:

$$G_{tensile}(P_w, \mathbf{X}) = T - \sigma'_\theta(P_w, \mathbf{X}), \tag{26}$$

Respectively, for the shear failure of wellbore using the Jeager model as defined in Eqs. 18 and 19, we adopt the following second LSF:

$$G_{shear}(P_w, \mathbf{X}) = \mathrm{Max}\begin{cases} -\dfrac{(\sigma'_r - \sigma'_\theta)}{2} - \dfrac{(\sigma'_r + \sigma'_\theta)\sin(\varphi_i)}{2} + C_i\cos(\varphi_i) \\ -\dfrac{(\sigma'_r - \sigma'_\theta)\sin(2\theta_w)}{2} - \left(\sigma'_r.\sin(\theta_w)^2 + \sigma'_\theta.\cos(\theta_w)^2\right)\tan(\varphi_w) + C_w \end{cases} \tag{27}$$

In Eqs. 26 and 27 all the random variables (i.e., anisotropic in-situ stress state, anisotropic poroelastic properties, anisotropic tensile or shear strength of rock mass) as defined previously are gathered in the vector $\mathbf{X}$ whilst the constant mud pressure P_w in wellbore plays the role of the design parameter. Note that, to simplify the presentation, the inclined angle θ is omitted in Eqs. 26 and 27 but keeping in mind that the two LSFs must be determined at the critical plane at which the value of each LSF $G(\mathbf{X})$ must be maximal. For the current problem that bases on the closed-form solutions, this critical plane (and hence the maximal value of $G(\mathbf{X})$) can be analytically evaluated. But, for the more complex problems in which the deterministic problem must be solved numerically, the post processing around well wall is necessary to determine this maximum value of $G(\mathbf{X})$ as well as critical position.[25]

In Fig. 15, the numerical applications of the Kriging metamodeling technique to determine the likelihood of success of two failure modes in wellbore are highlighted and compared with the results provided from the MCS. To simplify the presentation, only the undrained and permeable boundary cases are considered. In these calculations, the Kriging metamodel is built from 48 training points (generated by LHS technique) in the initial DoE while the same number of random samples (ten thousand realizations) as the direct MCS is chosen for the evaluation of failure probability by interpolation (Eq. (24)). In all the calculations, the number of iterations at convergence is less than 35. Thus, the total number of the direct evaluations of the wellbore response is about 83. A very good agreement between the Kriging metamodel and the MCS confirms the applicability and efficiency of this metamodeling technique on the probabilistic assessment of wellbore.

However, as observed in Fig. 15, for an arbitrary value of CL, the safe mud pressure window cannot be accessed directly by the Kriging-based stochastic analysis. Unlike the MCS in which the safe mud pressure window can be determined easily from the statistical processing of the exact results of wellbore response thanks to the direct evaluation of all random samples (ten thousand), in the Kriging metamodeling technique, the safe mud pressure window corresponding to a predefined CL must be calculated iteratively through an optimization procedure.[54] This problem, known also as the reliability-based design optimization of safe mud pressure window of wellbore using metamodeling technique will be discussed in our future work. Nevertheless, the proposition of the failure criteria and the adaptation with high accuracy of the Kriging metamodel in this study provide a useful tool for the probabilistic analysis of wellbore. Furthers, an extension in the future of this technique by accounting for the time-dependent effect allows treating the problem in different complex contexts such as the fully HM coupling in the transient state of the anisotropic rock as well as their interaction with the thermal and/or chemical phenomena. Combining with an appropriate optimization algorithm such as the Quantile Monte Carlo approach,[55,56] the Kriging metamodel allows a quick estimation of safe mud pressure window which is particularly important in wellbore design.

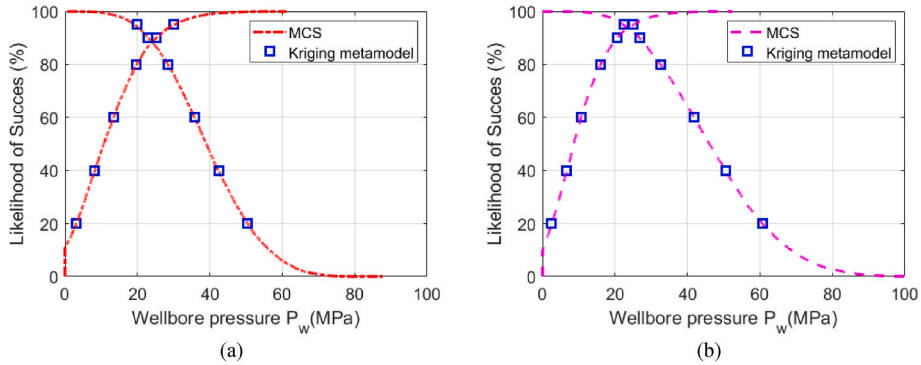

Fig. 15. Likelihood of success of mud pressure window calculated by Kriging metamodeling technique and MCS: permeable boundary (a), undrained case (b).

4. Conclusion

In this study, the investigation of the safe mud pressure window of the horizontal wellbore is conducted considering the combined effect of anisotropy and uncertainty, which has not been studied in the literature yet. For this aim, the deterministic results of the fracture and collapse pressures in the wellbore are derived using the available analytical solutions of stress state on the well wall and two well-known anisotropic models describing the tensile strength (the Nova and Zaninetti model) and shear strength (the single weakness plane model of Jaeger) of rock. Three cases are considered which describe the behavior of wellbore immediately after drilling (i.e., undrained problem) and at long term due to the steady-state fluid flow (permeable boundary case) or by ignoring the variation of initial pore pressure (i.e., impermeable boundary condition case).

The numerical applications are carried out for the VTI Tournemire shale rock whose hydro-mechanical properties are taken from the literature. The sensitivity analysis in this specific rock shows that the in-situ stress state is the most sensitive factor with respect to the safe mud pressure windows. It seems that the shear strength parameters (e.g., the cohesion, the friction angle) of the weak plane have more effect than the anisotropic elastic properties, which in turn affect more significantly than the tensile strength parameters. The effect of initial pore pressure, Biot coefficient and Biot modulus presents a moderate impact on the variation of mud weight windows. The stochastic analysis by MCS elucidates a strong uncertainty of the safe mud weight windows which are much narrower than the deterministic results and can be vanished beyond a critical value of the confidence level. It is worth noting that the results of safe mud pressure windows depend on the adopted hydraulically boundary condition at the circumference of well wall. Among the considered cases, the results show that the safe mud pressure window is the largest in the undrained case and narrowest when the steady fluid flow around the wellbore is accounted for. The safe mud pressure windows of the three cases are also calculated for the isotropic rock whose mechanical properties are extracted from the vertical direction of the VTI rock whilst the tensile and shear strengths corresponding to the ones of the bedding plane. In comparison with the initial anisotropic rock, the safe mud pressure windows of isotropic rock provide a moderate difference with higher values of both collapse and fracture pressures.

Finally, a proposition of the two limit state functions characterizing the tensile and shear failure modes allows us to adapt the Kriging metamodeling technique in the stochastic analysis of wellbore. The performance of this technique was demonstrated by comparing with the MCS. The study conducted in this work confirms the crucial role of uncertainty combined with anisotropic effect on the stability of wellbore whilst the Kriging metamodeling can provide an efficient tool for the probabilistic assessment of the safe mud pressure window.

Declaration of competing interest

The authors declare that they have no known competing financial interests or personal relationships that could have appeared to influence the work reported in this paper.

Acknowledgements

This research is funded by Vietnam National Foundation for Science and Technology Development (NAFOSTED), under grant number 105.99-2020.21.

Appendix A. Expression of radial and tangential stresses on the wellbore wall by accounting for the steady fluid flow

This appendix presents the closed-form solution of the principal (i.e. tangential and radial) stresses determined on the well wall by accounting for the variation of pore pressure in the steady state. This solution is synthetized from .[7]

The total stresses around the wellbore are expressed in the forms:

$$\begin{aligned}\sigma_x &= \sigma_x^{Ia} + \left(\sigma_x^{Ib} + \sigma_x^{II}\right) + \sigma_x^{Ipp} + \sigma_x^{Iph}\\ \sigma_y &= \sigma_y^{Ia} + \left(\sigma_y^{Ib} + \sigma_y^{II}\right) + \sigma_y^{Ipp} + \sigma_y^{Iph}\\ \tau_{xy} &= \tau_{xy}^{Ia} + \left(\tau_{xy}^{Ib} + \tau_{xy}^{II}\right) + \tau_{xy}^{Ipp} + \tau_{xy}^{Iph}\end{aligned} \tag{A1}$$

in which

$$\sigma_x^{Ia} = \sigma_h, \quad \sigma_y^{Ia} = \sigma_v, \quad \tau_{xy}^{Ia} = \tau_{vh} \tag{A2}$$

The solution of total stresses with superscripts Ib and II are derived from:

$$\sigma_x^{Ib} + \sigma_x^{II} = 2\mathrm{Re}\left[\mu_1^2\Phi_1{}' + \mu_2^2\Phi_2{}'\right], \quad \sigma_y^{Ib} + \sigma_y^{II} = 2\mathrm{Re}\left[\Phi_1{}' + \Phi_2{}'\right], \quad \tau_{xy}^{Ib} + \tau_{xy}^{II} = -2\mathrm{Re}\left[\mu_1\Phi_1{}' + \mu_2\Phi_2{}'\right], \tag{A3}$$

In Eq. (A3), the two potentials Φ_1, Φ_2 and their derivatives are expressed in the form:

$$\begin{aligned}\Phi_1 &= \Phi_1^{Ib} + \Phi_1^{II} = \frac{1}{2}\frac{r_0}{\mu_1 - \mu_2}\left[(1 - i\mu_2)\tau_{vh} + \mu_2\sigma_v - i\sigma_h + r_0P_w(\mu_2 - i)\right]\frac{1}{\zeta_1},\\ \Phi_2 &= \Phi_2^{Ib} + \Phi_2^{II} = \frac{1}{2}\frac{r_0}{\mu_2 - \mu_1}\left[(1 - i\mu_1)\tau_{vh} + \mu_1\sigma_v - i\sigma_h + r_0P_w(\mu_1 - i)\right]\frac{1}{\zeta_2},\\ \Phi_1' &= \frac{A_1 + i.B_1}{C_1 + i.D_1} = \frac{(A_1.C_1 + B_1.D_1) + i(B_1.C_1 - A_1.D_1)}{C_1^2 + D_1^2},\\ \Phi_2' &= \frac{A_2 + i.B_2}{C_2 + i.D_2} = \frac{(A_2.C_2 + B_2.D_2) + i(B_2.C_2 - A_2.D_2)}{C_2^2 + D_2^2}\end{aligned} \tag{A4}$$

Thus:

$$\sigma_x^{Ib}+\sigma_x^{II}=2\left[\frac{\left(\mu_{11}^2-\mu_{12}^2\right)(A_1.C_1+B_1.D_1)-2\mu_{11}\mu_{12}(B_1.C_1-A_1.D_1)}{C_1^2+D_1^2}+\frac{\left(\mu_{21}^2-\mu_{22}^2\right)(A_2.C_2+B_2.D_2)-2\mu_{21}\mu_{22}(B_2.C_2-A_2.D_2)}{C_2^2+D_2^2}\right],$$
$$\sigma_y^{Ib}+\sigma_y^{II}=2\left[\frac{A_1.C_1+B_1.D_1}{C_1^2+D_1^2}+\frac{A_2.C_2+B_2.D_2}{C_2^2+D_2^2}\right], \tag{A5}$$
$$\tau_{xy}^{Ib}+\tau_{xy}^{II}=-2\left[\frac{\mu_{11}(A_1.C_1+B_1.D_1)-\mu_{12}(B_1.C_1-A_1.D_1)}{C_1^2+D_1^2}+\frac{\mu_{21}(A_2.C_2+B_2.D_2)-\mu_{22}(B_2.C_2-A_2.D_2)}{C_2^2+D_2^2}\right]$$

where

$$\begin{aligned}
A_1 &= [P_w(\mu_{22}-1)-\sigma_h+\mu_{22}.\sigma_v-\mu_{21}.\tau_{vh}]\cos\theta-[\mu_{21}(P_w+\sigma_v)+(1+\mu_{22})\tau_{vh}]\sin\theta,\\
A_2 &= [P_w(1-\mu_{12})+\sigma_h-\mu_{12}.\sigma_v+\mu_{11}.\tau_{vh}]\cos\theta+[\mu_{11}(P_w+\sigma_v)+(1+\mu_{12})\tau_{vh}]\sin\theta,\\
B_1 &= -[\mu_{21}(P_w+\sigma_v)+(1+\mu_{22})\tau_{vh}]\cos\theta+[P_w(1-\mu_{22})+\sigma_h-\mu_{22}.\sigma_v+\mu_{21}.\tau_{vh}]\sin\theta,\\
B_2 &= [\mu_{11}(P_w+\sigma_v)+(1+\mu_{12})\tau_{vh}]\cos\theta+[P_w(\mu_{12}-1)-\sigma_h+\mu_{12}.\sigma_v-\mu_{11}.\tau_{vh}]\sin\theta,\\
C_1 &= 2\left[\mu_{11}^2-\mu_{11}\mu_{21}+\mu_{12}(\mu_{22}-\mu_{12})\right]\cos\theta+2(\mu_{21}-\mu_{11})\sin\theta,\\
C_2 &= 2\left[\mu_{22}^2-\mu_{12}\mu_{22}+\mu_{21}(\mu_{11}-\mu_{21})\right]\cos\theta+2(\mu_{21}-\mu_{11})\sin\theta,\\
D_1 &= 2[2\mu_{11}\mu_{12}-\mu_{12}\mu_{21}-\mu_{11}\mu_{22}]\cos\theta+2(\mu_{22}-\mu_{12})\sin\theta,\\
D_2 &= 2[2\mu_{11}\mu_{12}-\mu_{12}\mu_{21}-\mu_{11}\mu_{22}]\cos\theta+2(\mu_{22}-\mu_{12})\sin\theta,
\end{aligned} \tag{A6}$$

The other solutions of stress state are written as:

$$\begin{aligned}
\sigma_x^{Ipp} &= \Sigma_x=(p_0-p_{ff})\left(2N_{12}.\mu_{11}.\mu_{12}+N_{11}.\left(\mu_{12}^2-\mu_{11}^2\right)+N_{21}.\left(\mu_{22}^2-\mu_{21}^2\right)+2N_{22}.\mu_{21}.\mu_{22}+\eta.\mu_{w2}^2\right);\\
\sigma_y^{Ipp} &= \Sigma_y=-(p_0-p_{ff})(N_{11}+N_{21}+\eta);\\
\tau_{xy}^{Ipp} &= T_{xy}=-(p_0-p_{ff})(N_{12}.\mu_{12}-N_{11}.\mu_{11}+N_{22}.\mu_{22}-N_{21}.\mu_{21});
\end{aligned} \tag{A7}$$

and:

$$\sigma_x^{Iph}=2\mathrm{Re}\left[\mu_1^2.\Phi_1^{Iph'}+\mu_2^2.\Phi_2^{Iph'}\right]=2\frac{\left(\mu_{11}^2-\mu_{12}^2\right)(E_1.C_1+F_1.D_1)-2\mu_{11}\mu_{12}(F_1.C_1-E_1.D_1)}{C_1^2+D_1^2}+2\frac{\left(\mu_{21}^2-\mu_{22}^2\right)(E_2.C_2+F_2.D_2)-2\mu_{21}\mu_{22}(F_2.C_2-E_2.D_2)}{C_2^2+D_2^2},$$
$$\sigma_y^{Iph}=2\mathrm{Re}\left[\Phi_1^{Iph'}+\Phi_2^{Iph'}\right]=2\left[\frac{E_1.C_1+F_1.D_1}{C_1^2+D_1^2}+\frac{E_2.C_2+F_2.D_2}{C_2^2+D_2^2}\right], \tag{A8}$$
$$\tau_{xy}^{Iph}=-2\mathrm{Re}\left[\mu_1.\Phi_1^{Iph'}+\mu_2.\Phi_2^{Iph'}\right]=-2\frac{\mu_{11}(A_1.C_1+B_1.D_1)-\mu_{12}(B_1.C_1-A_1.D_1)}{C_1^2+D_1^2}+2\frac{\mu_{21}(A_2.C_2+B_2.D_2)-\mu_{22}(B_2.C_2-A_2.D_2)}{C_2^2+D_2^2}$$

The parameters E_1, E_2, F_1, F_2 are defined as:

$$\begin{aligned}
E_1 &= -\left(\Sigma_x+\mu_{21}.T_{xy}-\mu_{22}.\Sigma_y\right)\cos\theta-\left(\mu_{21}.\Sigma_y+(1+\mu_{22})T_{xy}\right)\sin\theta,\\
E_2 &= \left(\Sigma_x+\mu_{11}.T_{xy}-\mu_{12}.\Sigma_y\right)\cos\theta+\left(\mu_{11}.\Sigma_y+(1+\mu_{12})T_{xy}\right)\sin\theta,\\
F_1 &= -\left(\mu_{21}.\Sigma_y+(1+\mu_{22})T_{xy}\right)\cos\theta+\left(\Sigma_x+\mu_{21}.T_{xy}-\mu_{22}.\Sigma_y\right)\sin\theta,\\
F_2 &= \left(\mu_{11}.\Sigma_y+(1+\mu_{12})T_{xy}\right)\cos\theta-\left(\Sigma_x+\mu_{11}.T_{xy}-\mu_{12}.\Sigma_y\right)\sin\theta
\end{aligned} \tag{A9}$$

The parameters μ_{11}, μ_{21} and μ_{12}, μ_{22} in Eqs. (A5 to A9) are the real and imaginary part of two complex roots μ_1, μ_2 (with positive imaginary part) of the characteristic equation:

$$s_{11}\mu^4+(2s_{12}+s_{33})\mu^2+s_{22}=0 \tag{A10}$$

In Eq. (A7) the real parameter η is calculated from:

$$\eta=-\frac{\beta_1\mu_w^2+\beta_2}{s_{11}\mu_w^4+(2s_{12}+s_{33})\mu_w^2+s_{22}} \tag{A11}$$

and $\mu_{w2}=\sqrt{k_x/k_y}$ is the imaginary part of the purely imaginary parameter μ_w. The other parameters N_{11}, N_{21} and N_{12}, N_{22} are the real and imaginary part of two complex constants N_1, N_2 which are determined from the following system of equations (see Appendix A of[7]):

$$\begin{aligned}
&\mathrm{Im}\left[\mu_1^2N_1+\mu_2^2N_2+\mu_w^2\eta\right]=0,\\
&\mathrm{Im}[N_1+N_2+\eta]=0,\\
&\mathrm{Im}[\mu_1N_1+\mu_2N_2+\mu_w\eta]=0,\\
&\mathrm{Im}[q_1N_1+q_2N_2+q_w\eta-\beta_2/\mu_w]=0
\end{aligned} \tag{A12}$$

In case that the roots μ_1, μ_2 of the characteristic equation are purely imaginary, the following expressions of N_1, N_2 are derived in ([20]):

$$\begin{aligned}
N_{11} &= -\frac{-(\beta_2+\eta q_{w2}\mu_{w2})\mu_{22}+\eta q_{22}\mu_{w2}^2}{(q_{22}\mu_{12}-q_{12}\mu_{22})\mu_{w2}},\quad N_{12}=0,\\
N_{21} &= -\frac{(\beta_2+\eta q_{w2}\mu_{w2})\mu_{12}-\eta q_{12}\mu_{w2}^2}{(q_{22}\mu_{12}-q_{12}\mu_{22})\mu_{w2}},\quad N_{22}=0,\\
p_i &= s_{11}\mu_i^2+s_{12},\quad q_i=s_{12}\mu_i+\frac{s_{22}}{\mu_i},\quad (i=1,2,w)
\end{aligned} \tag{A13}$$

Finally, the effective tangential and radial stress on the wall of wellbore are deduced as follows by using the Biot's theory:

$$\sigma'_x = \sigma_x + \alpha_x p_0, \quad \sigma'_y = \sigma_y + \alpha_y p_0,$$
$$\sigma'_\theta = \frac{\sigma'_x + \sigma'_y}{2} - \frac{\sigma'_x - \sigma'_y}{2}\cos 2\theta - \tau_{xy}\sin 2\theta, \tag{A14}$$
$$\sigma'_r = \frac{\sigma'_x + \sigma'_y}{2} + \frac{\sigma'_x - \sigma'_y}{2}\cos 2\theta + \tau_{xy}\sin 2\theta,$$

with $p_0 = P_w$ (case permeable boundary) or $p_0 = p_{ff}$ (case impermeable boundary).

Appendix B. Closed-form solution of stress state around wellbore in the undrained case

For the undrained case, the behavior of wellbore is purely mechanical by accounting for the effect of initial and excess pore pressure in the calculation of effective stress state. Thus, with respect to the previous case defined in Appendix A, only the solution of problem I, Ib and II are necessary.

The solution of problem I as expressed in Eq. (A2) is remained as it represents the initial stress state around wellbore before excavation. For the excavation problem with wellbore pressure P_w (problem Ib and II), by substituting the total stress defined in Eq. (A3) in Eq. (10) the following excess pore pressure can be obtained:

$$\Delta p = 2\mathrm{Re}\left[-\frac{\beta_1\mu_1^2 + \beta_2}{\beta_3}\Phi_1' - \frac{\beta_1\mu_2^2 + \beta_2}{\beta_3}\Phi_2'\right], \tag{B1}$$

The expressions of the two potentials Φ_1, Φ_2 and their derivatives are similar with ones defined in Eq. (A4) but the complex roots μ_1, μ_2 are now determined from the following characteristic equation (see also Bobet and Yu, 2015):

$$A_{11}\mu^4 + (2A_{12} + A_{33})\mu^2 + A_{22} = 0, \tag{B2}$$

where:

$$A_{11} = s_{11} - \frac{\beta_1^2}{\beta_3}, \quad A_{12} = s_{12} - \frac{\beta_1\beta_2}{\beta_3}, \quad A_{33} = s_{33}, \quad A_{22} = s_{22} - \frac{\beta_2^2}{\beta_3}, \tag{B3}$$

Thus, one can deduce the effective tangential and radial stress on the wall of wellbore as defined in Eq. (A14) in which $p_0 = p_{ff} + \Delta p$.

Appendix C. Analytical solutions of stress state around the wellbore in the isotropic rock

For the comparison purpose, the analytical solutions of stress state and the safe mud pressure windows of wellbore in the isotropic rock, which have been derived since the long time, are rewritten in this appendix. Following that, the solution for the case of wellbore in the dry rock will be firstly captured and then extended in the other cases (i.e., permeable boundary, impermeable boundary, and undrained rocks) as considered in the anisotropic part. The interested reader can refer to the well-known contributions ([5,13,57]) for more details of the developments of these solutions.

- Case of dry rock:

$$\begin{aligned}
&\sigma_\theta = \sigma_v^{ff} + \sigma_h^{ff} + P_w - 2\left(\sigma_h^{ff} - \sigma_v^{ff}\right)\cos(2\theta);\\
&\sigma_r = -P_w;\\
&\sigma'_\theta = \sigma_\theta;\\
&\sigma'_r = \sigma_r;
\end{aligned} \tag{C1}$$

- Case of impermeable boundary (i.e., constant pore pressure in the rock mass):

$$\begin{aligned}
&\sigma_\theta = \sigma_v^{ff} + \sigma_h^{ff} + P_w - 2\left(\sigma_h^{ff} - \sigma_v^{ff}\right)\cos(2\theta);\\
&\sigma_r = -P_w;\\
&\sigma'_\theta = \sigma_\theta + \alpha.p_{ff};\\
&\sigma'_r = \sigma_r + \alpha.p_{ff};
\end{aligned} \tag{C2}$$

- Case of permeable boundary:

$$\begin{aligned}
&\sigma_\theta = \sigma_v^{ff} + \sigma_h^{ff} + P_w - 2\left(\sigma_h^{ff} - \sigma_v^{ff}\right)\cos(2\theta) - 2\frac{\alpha(1-2\nu)}{2(1-\nu)}\left(P_w - p_{ff}\right);\\
&\sigma_r = -P_w;\\
&\sigma'_\theta = \sigma_\theta + \alpha.P_w;\\
&\sigma'_r = \sigma_r + \alpha.P_w;
\end{aligned} \tag{C3}$$

- Undrained case:

$$\begin{aligned}
&\sigma_\theta = \sigma_v^{ff} + \sigma_h^{ff} + P_w - 2\left(\sigma_h^{ff} - \sigma_v^{ff}\right)\cos(2\theta);\\
&\sigma_r = -P_w;\\
&\delta p = \frac{\alpha.M}{\lambda + \alpha^2.M + G}\left(\sigma_h^{ff} - \sigma_v^{ff}\right)\cos(2\theta);\\
&\sigma_\theta^{'} = \sigma_\theta + \alpha.\left(p_{ff} + \delta p\right);\\
&\sigma_r^{'} = \sigma_r + \alpha.\left(p_{ff} + \delta p\right);
\end{aligned} \tag{C4}$$

In Eq. (C4), λ and G are the two Lamé parameters.

It is important to remind here that the compressive stress is negative in this study while the wellbore and pore pressures are positives.

From these explicit expressions of effective stresses in the well wall, the fracture initiation pressure and collapse pressure can be deduced without difficulty using the following conditions:

$$\begin{aligned}
&\sigma^{'}{}_\theta = T,\\
&\frac{\left(\sigma_r^{'} - \sigma_\theta^{'}\right)}{2} + \frac{\left(\sigma_r^{'} + \sigma_\theta^{'}\right)\sin(\varphi)}{2} - C\cos(\varphi) = 0,
\end{aligned} \tag{C5}$$

where T is the tensile strength while C and φ are the Mohr Coulomb parameters of the isotropic rock.

References

1 Fjaer E, Holt RM, Raaen AM, Risnes R. *Petroleum Related Rock Mechanics*. second ed. Developments in Petroleum Science: Elsevier; 2008.
2 Aadnoy SB, Looyeh R. *Petroleum Rock Mechanics: Drilling Operation and Well Design*. Amsterdam: Elsevier publication; 2010.
3 Darvishpour A, Cheraghi SM, Wood DA, Ghorbani H. Wellbore stability analysis to determine the safe mud weight window for sandstone layers. *Petrol Explor Dev*. 2019; 46:1031–1038.
4 Gupta D, Zaman M. Stability of borehole in a geologic medium including the effects of anisotropy. *Appl Math Mech*. 1999;20:837–866.
5 Zhang J. Borehole stability analysis accounting for anisotropies in drilling to weak bedding planes. *Int J Rock Mechan Min Sci*. 2013;60:160–170.
6 Kanfar MF, Chen Z, Rahman SS. Risk-controlled wellbore stability analysis in anisotropic formations. *J Petrol Sci Eng*. 2015;134:214–222.
7 Do DP, Tran NH, Hoxha D, Dang HL. Assessment of the influence of hydraulic and mechanical anisotropy on the fracture initiation pressure in permeable rocks using a complex potential approach. *Int J Rock Mech Min Sci*. 2017;100:108–123.
8 Do DP, Tran NH, Dang HL, Hoxha D. Closed-form solution of stress state and stability analysis of wellbore in anisotropic permeable rocks. *Int J Rock Mechan Min Sci*. 2019; 113:11–23.
9 Aadnoy BS. Stress around horizontal boreholes drilled in sedimentary rocks. *J Petrol Sci Eng*. 1989;2:349–360.
10 Hefny AM, Lo KY. Analytical solutions for stresses and displacements around tunnels driven in cross-anisotropic rocks. *Int J Num Anal Method Geomech*. 1999;23:161–177.
11 Lekhnitskii SG. *Theory of Elasticity of an Anisotropic Elastic Body*. San Francisco: Holden-Day; 1963. Inc.
12 Lekhnitskii SG. *Anisotropic Plates*. New York: Gordon and Breach; 1968.
13 Aadnoy BS. Modeling of the stability of highly inclined boreholes in anisotropic rock formations. *SPE Drill Eng*. 1988;3:259–268.
14 Setiawan NB, Zimmerman RW. Wellbore breakout prediction in transversely isotropic rocks using true-triaxial failure criteria. *Int J Rock Mechan Min Sci*. 2018; 112:313–322.
15 Amadei B. *Rock Anisotropy and the Theory of Stress Measurements*. Berlin: Springer-Verlag; 1983.
16 Aadnoy B, Hareland G, Kustamsi A, de Freitas T, Hayes J. *Borehole Failure Related to Bedding Plane*, 43rd US Rock Mechanics Symposium & 4th US-Canada Rock Mechanics Symposium. Asheville: North Carolina; June 2009:9–106. Paper ARMA.
17 Liu X, Zeng W, Liang L, Lei M. Wellbore stability analysis for horizontal wells in shale formations. *J Nat Gas Sci Eng*. 2016;31:1–8.
18 Ma T, Zhang QB, Chen P, Yang C, Zhao J. Fracture pressure model for inclined wells in layered formations with anisotropic rock strengths. *J Petrol Sci Eng*. 2017;149: 393–408.
19 Tran NH. *Hydro-mechanical Behavior of Deep Tunnels in Anisotropic Poroelastic Medium*. PhD dissertation. France: University of Orléans; 2016.
20 Tran NH, Do DP, Hoxha D. A closed-form hydro-mechanical solution for deep tunnels in elastic anisotropic rock. *Eur J Environ Civ Eng*. 2017:1–17.
21 Do DP, Tran NH, Hoxha D. Behavior of horizontal borehole in anisotropic poro-elastic media with transient fluid flow: a closed-form solution based on the complex potential approach. In: *Proceedings of the Sixth Biot Conference on Poromechanics*. July 2017:9–13. Paris.
22 Vu MN, Guayacán Carrillo LM, Armand G. Excavation induced over pore pressure around drifts in the Callovo-Oxfordian claystone. *Eur J Environ Civ Eng*. 2020:1–16. https://doi.org/10.1080/19648189.2020.1784800.
23 Do DP, Tran NT, Mai VT, Hoxha D, Vu MN. Time-dependent reliability analysis of deep tunnel in the viscoelastic Burger rock with the sequential installation of liners. *Rock Mech Rock Eng*. 2019;53:1259–1285.
24 Do DP, Vu MN, Tran NT, Armand G. Closed-form solution and reliability analysis of deep tunnel supported by a concrete liner and a covered compressible layer within the viscoelastic Burger rock. *Rock Mech Rock Eng*. 2021;54:2311–2334.
25 Tran NT, Do DP, Hoxha D, Vu MN, Armand G. Kriging-based reliability analysis of the long-term stability of a deep drift constructed in the Callovo-Oxfordian claystone. *J Rock Mech Geotech Eng*. 2021. https://doi.org/10.1016/j.jrmge.2021.06.009.
26 Ottesen RH, Zheng RH, McCann RC. Borehole stability assessment using quantitative risk analysis. In: *SPE/IADC Drilling Conference*. March 1999. Paper SPE-52864-MS.
27 Moos D, Peska P, Finkbeiner T, Zoback M. Comprehensive wellbore stability analysis utilizing quantitative risk assessment. *J Petrol Sci Eng*. 2003;38:97–109.
28 Gholami R, Rabiei M, Rasouli V, Aadnoy BS, Fakhari N. Application of quantitative risk assessment in wellbore stability analysis. *J Petrol Sci Eng*. 2015;135:185–200.
29 Mondal S, Chatterjee R. Quantitative risk assessment for optimum mud weight window design: a case study. *J Petrol Sci Eng*. 2019;176:800–810.
30 Udegbunam JE, Aadnoy BS, Fjelde KK. Uncertainty evaluation of wellbore stability model predictions. *J Petrol Sci Eng*. 2014;124:254–263.
31 Eshiet KII, Sheng Y. The performance of stochastic designs in wellbore drilling operations. *Petrol Sci*. 2018;15:335–365.
32 Zhang L, Bian Y, Zhang S, Yan Y. A new analytical model to evaluate uncertainty of wellbore collapse pressure based on advantageous synergies of different strength criteria. *Rock Mech Rock Eng*. 2019;52:2649–2664.
33 Al-Ajmi AM, Al-Harthy MH. Probabilistic wellbore collapse analysis. *J Petrol Sci Eng*. 2010;74:171–177.
34 Nino FAP. Wellbore stability analysis based on sensitivity and uncertainty analysis. In: *SPE Annual Technical Conference and Exhibition*. September 2016. Dubai, UAE. Paper SPE-184480-STU.
35 Ma Y, Yu R. New analytical methods to evaluate uncertainty of wellbore stability. *J Petrol Sci Eng*. 2019;180:268–277.
36 Ma T, Tang T, Chen P, Yang C. Uncertainty evaluation of safe mud weight window utilizing the reliability assessment method. *Energies*. 2019;12:942.
37 Han W, Yan Y, Yan X. Uncertainty and sensitivity analysis of in-situ stress in deep inclined strata. *Geotech Geol Eng*. 2020;38:2699–2712.
38 Zhang J, Bai M, Roegiers JC. Dual-porosity poroelastic analysses of wellbore stability. *Int J Rock Mechan Min Sci*. 2003;40:473–483.
39 Bobet A, Yu H. Stress field near the tip of a crack in a poroelastic transversely anisotropic saturated rock. *Eng Fract Mech*. 2015;141:1–18.
40 Nova R, Zaninetti A. An investigation into the tensile behavior of a schistose rock. *Int J Rock Mechan Min Sci Geomech*. 1990;27:231–242.
41 Lee YK, Pietruszczak S. Tensile failure criterion for transversely isotropic rocks. *Int J Rock Mechan Min Sci*. 2015;79:205–215.
42 Jaeger JC. Shear failure of anisotropic rocks. *Geol Mag*. 1960;97:65–72.
43 Pietruszczak S, Pande GN. Description of soil anisotropy based on multi-laminate framework. *Int J Num Anal Methods Geomech*. 2001;25:197–206.
44 Pietruszczak S, Mroz Z. On failure criteria for anisotropic cohesive-frictional materials. *Int J Num Anal Methods Geomech*. 2001;25:509–524.
45 Mroz Z, Maciejewski J. Failure criteria of anisotropically damaged materials based on the critical plane concept. *Int J Numer Anal Method Geol*. 2002;26:407–431.
46 Jaeger JC, Cook NGW, Zimmerman W. *Fundamentals of Rock Mechanics*. fourth ed. Blackwell Publishing; 2007.
47 Chen X, Yang Q, Qui KB, Feng JL. An anisotropic strength criterion for jointed rock masses and its application in wellbore stability analyses. *Int J Num Anal Methods Geomech*. 2008;32:607–631.
48 Aadnoy BS. Quality assurance of wellbore stability analyses. In: *SPE/IADC Drilling Conference and Exhibition*. March 2011. Amsterdam, The Netherlands. Paper SPE-140205-MS.
49 Niandou HJ. *Etude du comportement rhéologique et modélisation de l'argilite de Tournemire. Application à la stabilité d'ouvrages souterrains (in French)*. PhD dissertation. 1994. Université des Sciences et Technologies de Lille, France.

50 Niandou HJ, Shao JF, Henry JP, Fourmaintraux D. Laboratory investigation of the mechanical behaviour of Tournemire shale. *Int J Rock Mech Min Sci*. 1997;34:3–16.
51 Cosenza P, Ghoreychi M, de Marsily G, Vasseur G, Violette S. Theoretical prediction of poroelastic properties of argillaceous rocks from in situ specific storage coefficient. *Water Resour Res*. 2002;38:1207.
52 Valès F, Nguyen Minh D, Gharbi H, Rejeb A. Experimental study of the influence of the degree of saturation on physical and mechanical properties in Tournemire shale (France). *Appl Clay Sci*. 2004;26:197–207.
53 Noiret A. *Contribution à la caractérisation du comportement géomécanique des roches couverture des réservoirs pétroliers (in French)*. PhD dissertation. 2009. Institut National Polytechnique de Lorraine, France.
54 Tran NT, Do DP, Hoxha D, Vu MN. Reliability-based design of deep tunnel excavated in the viscoelastic Burger rocks. In: *Geotech. Sustain. Infrastruct. Dev*. 2020:375–382. https://doi.org/10.1007/978-981-15-2184-3_48. Springer.
55 Moustapha M, Sudret B, Bourinet JM, Guillaume B. Quantile-based optimization under uncertainties using adaptive Kriging surrogate models. *Struct Multidiscip Optim*. 2016;54:1403–1421.
56 Do DP, Tran NT, Hoxha D, Vu MN, Armand G. Kriging-based optimization design of deep tunnel in the rheological Burger rock. *IOP Conf Ser Earth Environ Sci*. 2021:833, 012155.
57 Detournay E, Cheng AHD. Poroelastic response of a borehole in a non-hydrostatic stress field. *Int J Rock Mech Min Sci Geomech*. 1988;25:171–182.